EXPERIMENTAL STUDY OF DOWNWARD FLAME SPREAD RATE ON PMMA

by

Elmahadi A. Abulbaida

Submitted in partial fulfilment of the requirements
for the degree of Master of Applied Science

at

Dalhousie University
Halifax, Nova Scotia
May 2014

DEDICATION

To my mother, wife and lovely daughter for their love, support and encouragement which boost me in completing my work.

Table of Contents

List of Tables

List of Figures

Abstract

The purpose of this thesis is to experimentally study the downward flame spread rate and the angle of pyrolysis with different shapes of PMMA at different oxygen concentrations. The effect of sample shape is considered. The effect of oxygen concentration on flame spread rate and the angle of pyrolysis were studied.

A modified Critical Oxygen Index Apparatus was used to perform these experiments. The samples of PMMA were burned at different oxygen concentrations. A camera was used to capture the images of the burning and ImageJ software was also used to analyze the images.

The result of this work shows that the shape of the sample plays an important role in burning time, where the fuel with a large surface area takes a longer time to burn. It also showed that the velocity increases as the oxygen concentration increases, while the angle of pyrolysis decreases as the oxygen concentration increases for all of the sample shapes tested.

List of Symbols and Abbreviations Used

C_{pw}	Specific heat of fuel surface, kJ/kg
q_c	Heat conducted through the solid, J/s
q_{sb}	Heat transferred to the pyrolysis zone, J/s
q_{su}	Heat conducted through the gas, J/s
q_t	Total heat transferred to the solid, J/s
T_f	Flame temperature, K
T_g	Glass transition temperature, K
T_v	Vaporization temperature, K
T_{vap}	Vaporization temperature, K
T_∞	Ambient temperature, 298K
V_f	Flame spread rate, cm/s
V_g	Opposing flow velocity, cm/s
V_r	Relative velocity of oxidizer with respect to the flame, cm/s

Greek Symbols Used

ρ_w	Density of fuel surface, kg/m^3
λ	Thermal conductivity of solid fuel W/m.K
$\sqrt{2}$	Constant factor
$\frac{\pi}{4}$	Constant factor
2τ	Fuel thickness, mm
τ_{crit}	Transition criterion, mm
θ	Angle of pyrolysis, (deg.)

Abbreviations

N	Nitrogen
O	Oxygen
V	Flame spread rate, cm/s

Acknowledgements

I would like to thank my advisor Dr. Michael Pegg for his guidance and support throughout my thesis. I am grateful to Dr. Jan Haelssig for his advice and guiding during my research work and for being a member of my thesis committee, and Dr. Darrel Doman for being a member of my thesis committee too. I am also thankful to Mr. Matt Kujath for his guidance through my lab work.

Special thanks to my wife who gave me encouragement and support at tough time.

Chapter 1 Introduction

Three elements must be present for a fire to occur: fuel, heat and oxygen. These elements are known as the fire triangle. If any one of these elements is missing, a fire will not occur. Fuel is represented by anything solid, liquid or gas that is combustible; heat is required at a certain temperature or the fire will not ignite; and oxygen is needed both to start and continue a fire.

Other elements can act as an oxidizer, eg H_2O_2 or chloric acid, other gases such as nitrous oxide or Cl_2.

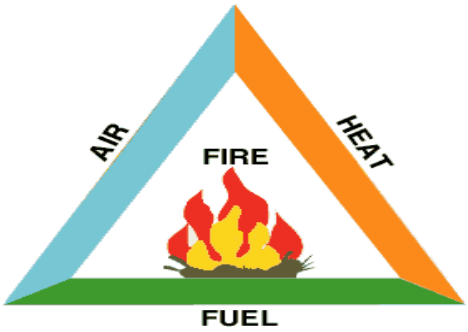

Figure 1.1 Fire triangle elements

1.1. Polymer Combustion Process

The combustion process for plastics is a complex phenomenon comprised of six stages:

1. Primary thermal - the primary thermal results from the ignition source heating the material to cause a rise in temperature. The temperature rise depends on the material being burned and the energy from the ignition source.
2. Primary chemical - when plastics begin to heat, they will degrade through the formation of a free radical that will occur under the influence of the ignition source. This process is similar to primary thermal but is more rapid because of the high energy that generates from the ignition source.
3. Polymer decomposition - polymer decomposition is the stage in which the plastics start to degrade into a lower molecular weight decomposition product.

4. Ignition - for combustible gases and liquids, the ignition source and sufficient oxygen (minimum 16% of the air) play an important role in burning after ignition occurs.
5. Combustion - the combustion occurs at or near the surface of plastic during the burning of gases. It can be described as a self-sufficient process if it produces sufficient energy. The methyl methacrylate repeat unit in brackets is the volatile fuel species when PMMA burns and it has the atomic composition $C_5H_8O_2$ so the balanced chemical equation for completely combustion of PMMA is:

   $C_5H_8O_2 + 6O_2 \longrightarrow 5CO_2 + 4H_2O$ (complete combustion).
6. Flame propagation - the type of plastic material involved in combustion plays an important role in flame propagation. In the combustion stage, flames may be produced that propagate and could be accompanied by the emission of smoke and toxic gases. (Zeus Industrial Products, 2005)

1.2. Poly(methylmethacrylate) (PMMA)

1.2.1. History

The first acrylic acid was created in 1843. In 1865, methacrylic acid was derived from acrylic and was formulated. The reaction between methacrylic acid and methanol results in the ester methyl methacrylate. Fittig and Paul (1877) discovered the process of polymerization, which turns MMA into PMMA. Otto Rohm (1933) patented and registered the brand name PLEXIGLAS. A few years later, (1936), the commercial production of acrylic safety glass began. (Jellinek, 1986)

1.2.2. PMMA preparation

PMMA is produced by emulsion polymerization, solution polymerization and bulk polymerization. Also, it is produced by radical polymerization (all commercial PMMA) is atactic and completely amorphous. (Nobuyuki, 1989)

$$C_4H_7NO \text{ (acetone cyanohydrin)} \xrightarrow[125\ ^\circ C]{H_2SO_4} C_4H_9NO_5S \text{ (Metha crylamide sulphate)} \xrightarrow[H_2O]{CH_3OH}$$

$$C_5H_8O_2 \text{ (Methyl methacrylate)} \xrightarrow{\text{Polymerization}} (C_5H_8O_2)_n \text{ (Poly (Metha methylacrylate))}$$

1.2.3. PMMA properties

Properties of polymethylmethacrylate (PMMA) are shown in table 1.1 below:

Table 1.1 Properties of PMMA

Property Name with Unit	PMMA
Density (kg/m^3)	1190
Enthalpy of Vaporization (kJ/kg)	941.04
Heat of Combustion (MJ/kg)	25.9
Oxygen Index	17-18
Molecular Formula	$(C_5O_2H_8)_n$

Properties of PMMA from (Feldman, 1991)

1.2.4. PMMA degradation

The glass transition temperature (T_g) of atactic PMMA is 105 °C and it is from 85°C to 165°C for all commercial grades of PMMA. PMMA homopolymer prepared by free radical polymerization is known to begin to degrade at 175 °C. Polymethylmethacrylate (PMMA) begins to degrade slowly at 220 °C and then 44-47% degrades in the temperature range 220-270 °C, but the degradation of PMMA is 100% when it is heated to 350 °C. Thermal degradation of PMMA at 300-400 °C is the chain radical reaction of depolymerization. The main volatile product of this process is methyl methacrylate (MMA). At a lower degradation temperature (340-361 °C) the mechanism of thermal degradation is initiated by a mixture of a chain scission process followed by depropagation. PMMA is degraded as a polymer that propagates to monomer as a result of thermal degradation up to 550 °C. (Jellinek, 1968)

The degradation of PMMA is a radical chain reaction that occurs in three irreversible steps (Nobuyuki, 1989) and (Jellinek, 1968):

- Initiation: PMMA degrades randomly into two radicals by the breakage of the bond in the position.

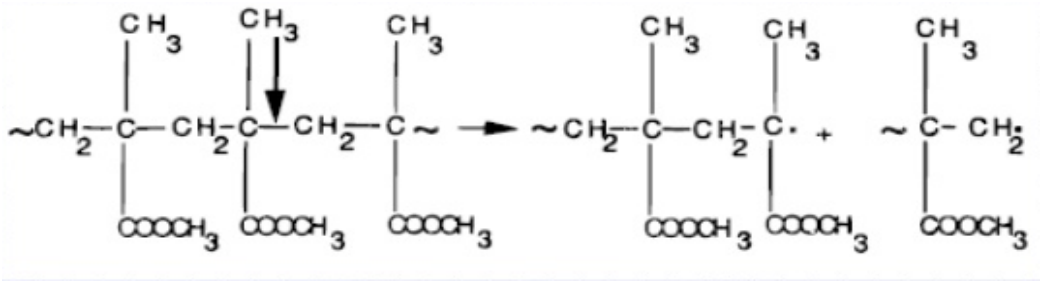

- Depropagation: The depropagation step consists of the production of the monomer from the newly created radicals.

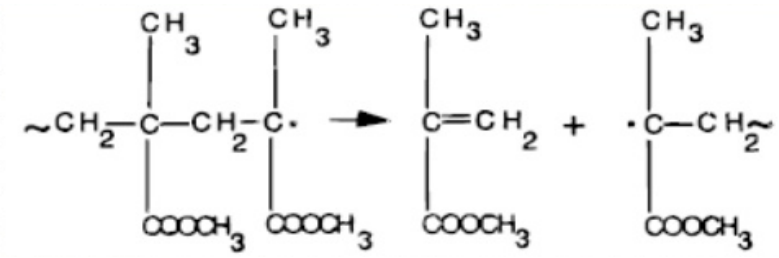

This is the reverse of the propagation step of polymerization.

- Termination: Termination occurs as a result of the interaction of the pair of radicals to reform a polymer. This model, with the stationary-state assumption for all radical concentration, leads to a rate equation that is first order in polymer concentration.

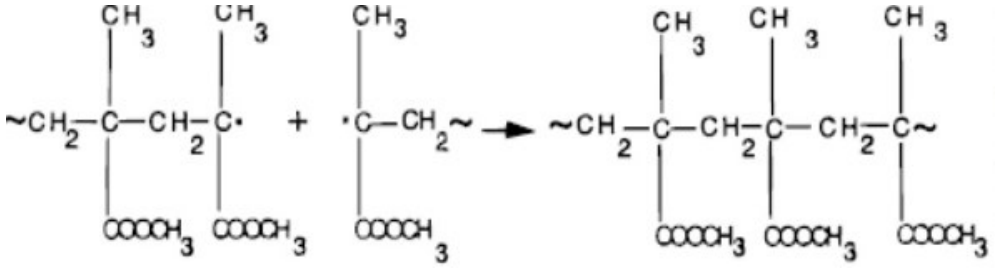

1.2.5 PMMA Common Uses

- Industrial uses: water tank liner, hand-held computer case, liquid chemical pump, conveyor rollers, soap dispensers hatch covers and bumper guards.
- Automotive Industry: lenses of exterior light, trunk release handle, master cylinder and dashboard lighting.

- Consumer Products: aquariums, motorcycle helmet lenses, paint, furniture, picture framing, umbrella clamps, cell phones antennas, bicycle air pump and AV wall outlets visors.
- Medical Applications: lens implants, hard contact lenses, dentures and filling.

1.3. Flame Spread

Flame spread, which is the rate of flame movement across a fuel surface, is an important topic related to fire safety. Flame spread is physically dependent on energy, momentum and species transfer in the region surrounding the flame reaction. This dependence must be considered when solving relevant problems in fire safety such as ignition and extinction. Flame spread can also be described as an exothermic reaction that involves fuel, which is present in any material, and an oxidizer that is present in the air and heat. The reaction would occur between the fuel and the oxidizer when the fuel is supplied with a sufficient amount of heat. The energy produced from the flame could be supplied in different modes to heat un - burnt fuel ahead of the flame depending on geometry of the system.

1.3.1. Downward Flame Spread

This is also called flame spread in opposed flow. This model of flame occurs when the flame spread direction is down and air flow opposes to the direction of propagation. The rates of flame spread are small in this case. Fig 1.2 shows a schematic of downward Flame spread.

The opposing flow velocity V_g could be due to buoyancy induced flow or forced flow. The oxidizer in this case is a mixture of Nitrogen (N_2) and Oxygen (O_2). The fuel undergoes pyrolysis when it is heated until its vaporization temperature T_v. An interaction occurs between the vaporized fuel and oxidizer product heat, and un-burnt fuel preheats by some of the heat that is produced from this interaction. The flame burns throughout the length of fuel by repeating this cycle of preheating, vaporization and combustion.

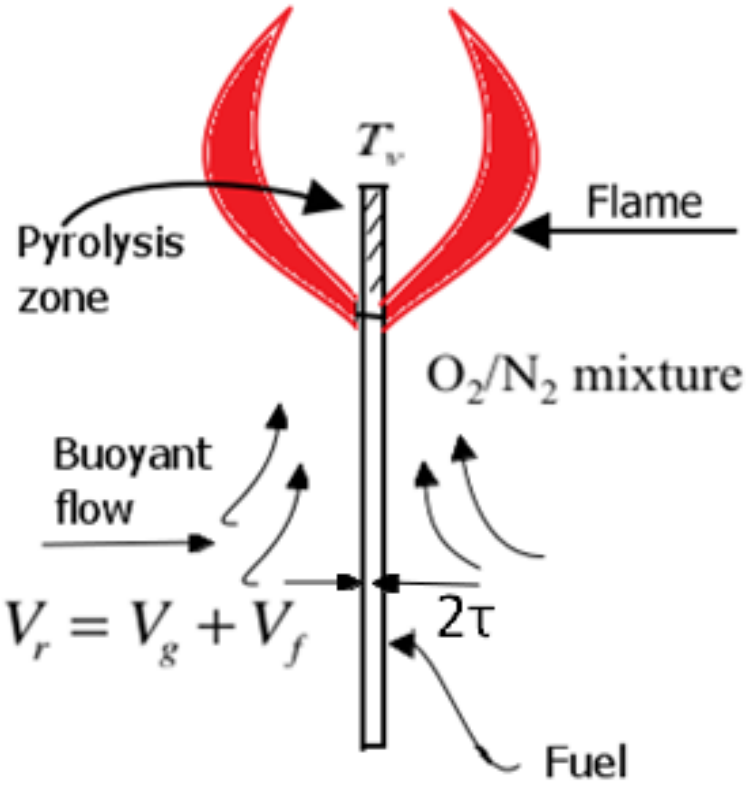

Figure 1.2 Schematic of downward Flame spread (Alghamdi, 2012)

Where:

V_f : Flame spread rate (cm/s)

V_g: Opposing flow velocity

V_r: Relative velocity of oxidizer with respect to the flame

T_v : Vaporization temperature (K)

2τ: Fuel thickness (mm)

There are three mechanisms by which heat may be transferred to the virgin material which are:

1. Radiation from the flame
2. Conduction or convection through the gas from the flame
3. Conduction through the solid

These three mechanisms are involved in heat transfer through downward flame spread and it is a challenge to determine which one of those mechanisms could control heat transfer through downward flame spread. An understanding of the dominant mode of heat transfer would ease the development of simplified and accurate description of flame spread. Therefore some experimental studies have been done on this subject.

Several studies have been done to determine the mode of heat transfer that controls the mechanism of flame spread. Hirano et al. (1974) calculated heat of flux at the fuel surface based on the measured temperature profile for flame spreading over paper sheets. He concluded that the heat conduction through the gas is the dominant mode of heat transfer through flame spread based on measuring temperature. Fernandez-Pello (1979) has done some energy balances for the gas and solid phases for flame spreading downward over thick and thin PMMA rods and he deduced that heat conduction through the gas is the dominant mode of heat transfer as the thickness of PMMA decreases. Fernandez-Pello and Hirano (1982) derived some results from some old work done by them, for flame spread downward over the surface of PMMA sheets of various thicknesses, as are shown in Fig. 1.3.

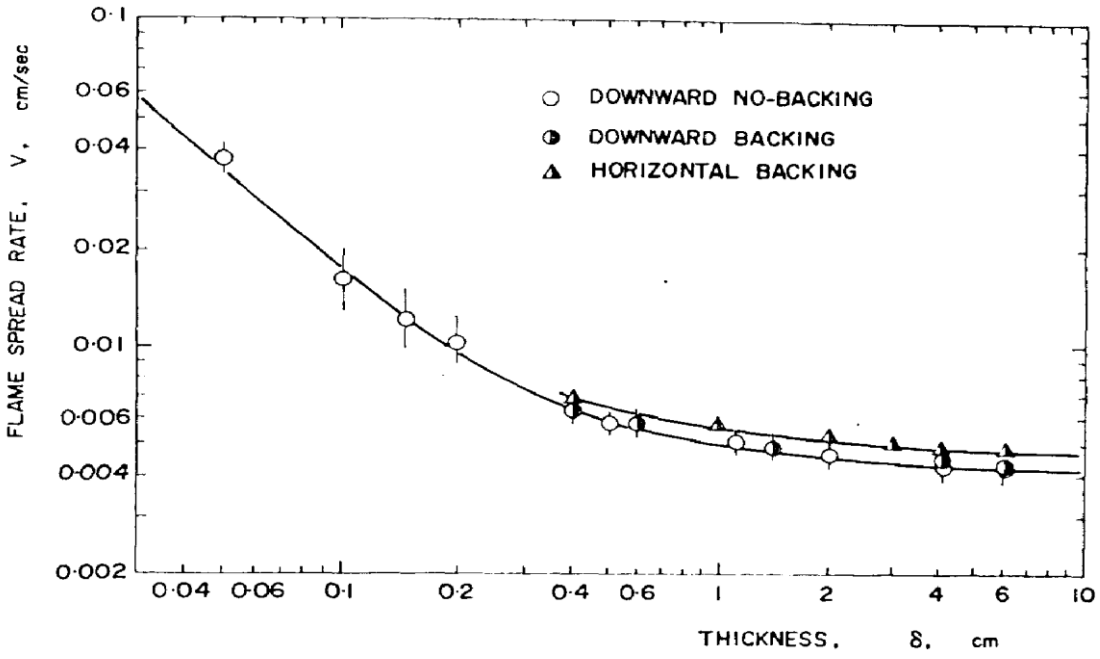

Figure 1.3 Variation with the solid thickness of the rate of flame spread over PMMA sheets, (Fernandez-Pello et al., 1982)

An inverse relationship is shown in Fig. 1.3 between the flame spread rate and fuel thickness to reach a constant value of flame spread rate as the thickness increases.

Also, they deduced different modes of heat transfer from the burning region of the solid to the virgin material for the flame spread downward over PMMA as shown in Fig. 1.4. The conclusion which they reached was based on the fuel thickness. They summarized that if the fuel thickness is smaller than 0.2 cm, the heat transfer to the un-burnt material is by conduction through the gas, but for fuel thickness larger than 0.2 cm, heat conduction through the solid is one of heat transfer ways. This conclusion is limited to some particular types of fuel, which leads them to say that no final conclusion, especially for thick fuel, can be reached until more different kinds of materials are tested.

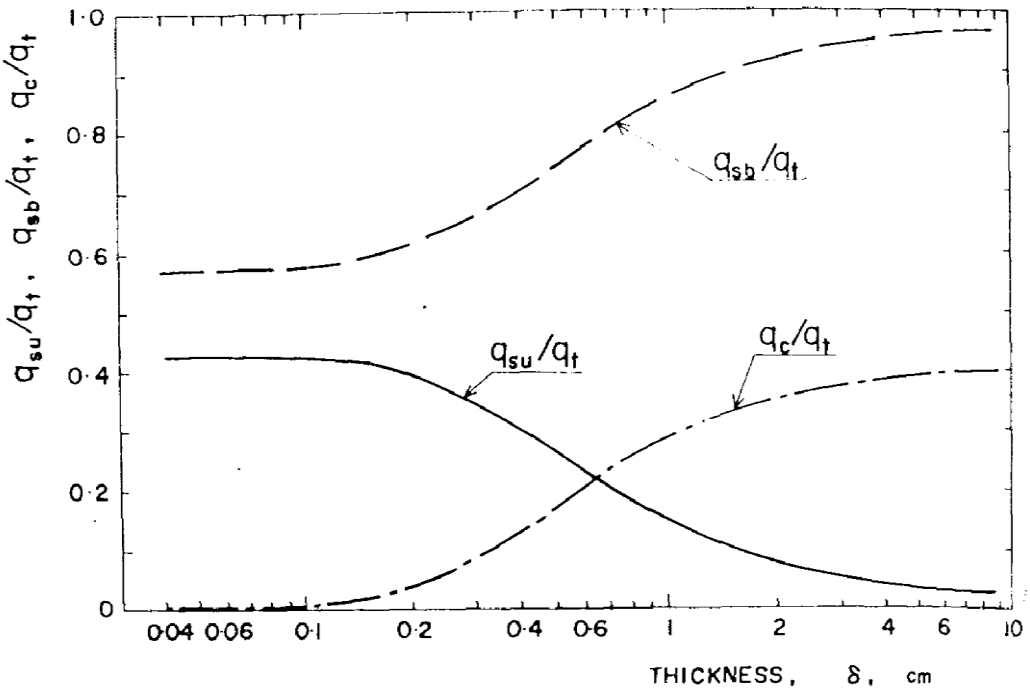

Figure 1.4 Shows variation with the solid thickness of the heat conducted from the flame to the un-burnt material for flame spreading over PMMA sheets, (Fernandez-Pello et al., 1982)

Where:

q_t= Total heat transferred to the solid; (J/s)

q_{su} = heat conducted through the gas; (J/s)

q_c = heat conducted through the solid; (J/s)

q_{sb} = heat transferred to the pyrolysis zone; (J/s)

There are other parameters that may also determine the spread rate, such as fuel type, fuel thickness, and geometrical orientation with respect to gravity, and ambient conditions.

The spread of the flame rate over fuel has been studied with regard to different orientations. The most common fuel orientations are upward, downward, horizontal topside, and horizontal underside as shown in Fig. 1.5. In upward flame spread, the solid fuel is kept vertical and the ignition would be provided from the bottom part of the fuel; hence, the flame would grow and move upward in an induced flow. In downward flame spread, the solid fuel is also kept vertical, but the ignition would be provided from the top. This makes the flame propagation move downward, as presented in Figure 1.5.

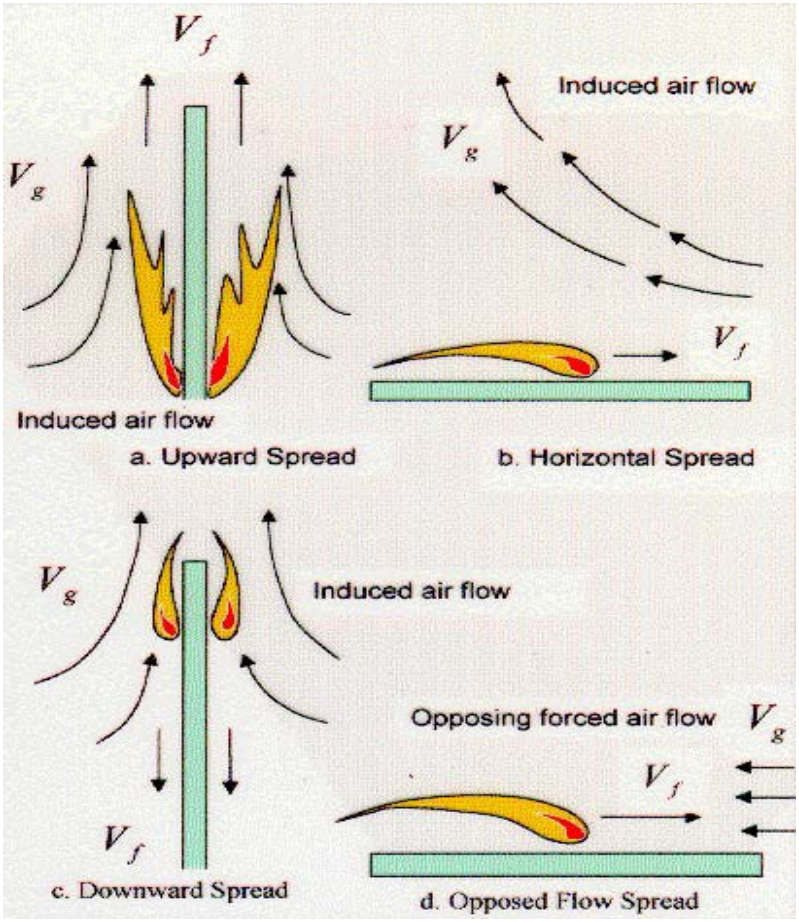

Figure 1.5 Different flame spread orientations, (Algamdi.,2012)

In a horizontal configuration, the fuel is oriented in a horizontal topside fire, which is opposite to the direction of the gas flow. However, in a horizontal underside situation, the fire moves in the same direction as the gas flow.

It is important to fully understand each simple case in order to grasp the complexity of flame spread. To date, numerous researchers have studied the phenomenon of vertical downward spreading flame over vertical slabs of polymethylmethacrylate (PMMA). PMMA is chosen as a fuel because its properties are well known and it is comparatively clean-burning fuel.

1.4 Objective

This experimental work on the downward burning of PMMA sheet extends previous studies by examining the effect of the ambient oxygen concentration on the spread rate and angle of pyrolysis.

The specific objectives were to study downward burning of sheets, square bars and rods of PMMA at different ambient oxygen concentrations (20, 21, 22, 24 and 26 %) to:

1. Measure the flame spread rate (cm/s) for different shapes of PMMA (sheets, square bars and rods) at different ambient oxygen concentrations (%).
2. Measure the angle of pyrolysis (deg.) at different ambient oxygen concentration.

Chapter 2 Literature Review

Many experimental, theoretical and modeling studies have been carried out to investigate the properties and characteristics of flame spread. deRis (1969) presented a theoretical formula based on the mathematical model of flame spread. He used the velocity of opposed flow spreading flame for a thermally thin and thick solid fuel, based on the neglecting of all physical properties (properties of fuel and gas were constant throughout th bgv bvgye analysis). The formula was in correlation with experimental data, especially for thin fuel.

$$\rho_w \, C_{Pw} \, \tau \, V_f \left(T_{vap} - T_\infty\right) = \sqrt{2} \, \lambda \left(T_f - T_{vap}\right) \qquad (1)$$

$$V_f = \sqrt{2} \left(\frac{T_f - T_{vap}}{T_{vap} - T_\infty}\right) \qquad (2)$$

Where;

ρ_w Density of fuel surface; kg/m^3

C_{Pw} Specific heat of fuel surface; kJ/Kg

τ Fuel half thickness, m

V_f Flame spread rate, m/s

T_{vap} Vaporization temperature K

T_∞ Ambient temperature, 298 K

T_f Flame temperature K

λ Thermal conductivity of solid fuel. W/m.K

$\sqrt{2}$ Constant Factor

Also, deRis(1969) described the laminar diffusion flame spreading process as:

"The hot flame heats the unburnt fuel bed subsequently vaporizes. The formulated model then treats the combustion as a diffusion flame for which the details of the reaction kinetics can be ignored by assuming infinite reaction rates."

Sirignano (1972) cities two negative factors in deRis's work which are: (i) thick fuel flame spread formula predicts that velocity of the gas is independent of the solid phase conductivity in direction of spread. He writes " one would intuitively expect that the spreading rate should depend very strongly on this conductivity increasing as it increases." Also, the absence of the solid-phase conductivity in the deRis formula was a sore point for other investigators. (ii) deRis vaporization temperature hypothesis is incorrect. Sirignano observes that vaporization

temperature depends on specific heat, chemical-kinetic constant, ambient pressure, ambient temperature, and fuel bed thickness. Therefore, the spread rate was studied under the simplifying assumption that combustion occurs in a heterogeneous reaction at the surface of the solid and a modified first-order Arrhenius law was used to estimate the rate of the reaction.

A similar analysis was done by Delichatsios (1986) for thermally thin materials. He applied the same formula as deRis(1969) but with a different constant factor. Delichatsios used $\frac{\pi}{4}$ instead of √2, which was in good agreement with the experimental result of the problem.

$$V_f = \frac{\pi}{4} \left(\frac{T_f - T_{vap}}{T_{vap} - T_\infty}\right) \qquad (3)$$

Paper index cards were used by Frey and Tien (1976) to perform downward and horizontal flame spread. In their experiments the spread rate was checked under low pressures and oxygen mole fractions, and temperature contour plots were produced for 10 and 3 psia pressure. The conclusion of the Frey study was an improved assumption of infinite rate chemical kinetics that became invalid near extinction conditions.

A laminar flame spread over flat PMMA surfaces was studied extensively by Fernandez-Pello and Williams (1975). Some results were also presented by thermocouple probing, photography, interferometry, radiometer measurements, gas sample chromatography and particle photography. The researchers reported that the heat transfer occurred via conduction through the solid phase.

Fernandez-Pello and Williams (1977) created an analytical model. From their experiments on downward flame spread, they concluded that the heat transfer maintaining the flame was controlled by heat conduction through the solid phase. While heat conduction could describe the flame spread process, the Arrhenius form was used for reactions of pyrolysis and gas, if the assumption of infinite rate chemical kinetics was neglected. Hence, the transition from thermally thin to thick was predicated by flame spread rate formula, which could also be used to calculate fuel thickness. However, a thermally thick fuel is the limiting case where the flame characteristics become independent of the fuel thickness while a thermally thin fuel is the limiting case where the temperature is constant across the thickness of the solid fuel and the flame spread rate is dependent on the thickness of the fuel.

Fernandez-Pello (1977) performed temperature measurement experiments on thick PMMA rods by using thermocouple probing and the velocity. He concluded that conduction was responsible for transferring heat through the solid phase.

Flame spread over a thermally thin solid fuel in uniform opposed flow in a steady state was developed by Frey and T'ien (1979). The theory was able to calculate the flame extinction limits, especially when the opposed velocity increased with decreases in pressure and ambient oxygen mass fraction as well.

In 1977, some analytical and experimental work on opposed flow flame spread over PMMA and cellulose fuel surface was done by Lastrina et al (1971). He showed that the flame spread velocity was measured as a function of pressure, oxygen concentration, fuel thickness and radiant heat, and that it opposed flow velocity. He concluded that the flame spread velocity increases with increasing the pressure and oxygen concentration. Furthermore, the flame velocity should increase linearly with the radiant heat, and the flame velocity also increases with increasing flow velocity, but the flame spreading velocity is inversely with the specimen thickness.

Parker (1972) performed experiments on thin cellulose index cards exposed to downward flame spread. An embedded thermocouple was used to obtain a surface temperature profile. Natural gas was piped in through an artificial flame spread burner, which was built to produce a stationary flame. The conclusion of his experiments was that the conduction through the gas phase was the dominant model of heat transfer to the virgin fuel.

Hirano (1974) used particle tracing methods and fine wire thermocouples to measure the temperature and velocity profiles for thin paper at different positions. His conclusion was that the gas phase contained about 80% heat transfer within 1 mm of the flame spread.

Fernandez-Pello et al. in (1981) studied the effect of opposed forced flow and ambient oxygen concentration on flame spread rate over thin and thick fuel (Paper and PMMA, respectively). They deduced that a direct relationship existed between the flame spread rate and the opposed flow velocity for thick PMMA at high oxygen concentrations, indicating that the flame spread rate increases as the opposed flow velocity increases. On the other hand, an inverse relationship also occurred between the flame spread rate and the opposed flow velocity for thin paper at all oxygen concentrations and for thick PMMA at low oxygen concentrations.

Thermally thick PMMA slabs were used as fuel by Ito and Kashiwagi (1988) to perform downward flame spread experiments. The interference fringes produced by holographic images were able to obtain the temperature measurements by counting them.

Bhattacharjee and Alterkirch (1992) conducted experiments and models to compare flame spread over thin fuel in microgravity. The experiments were conducted on board a space shuttle flight. From their experiments, the researchers concluded that the flame spread rate in microgravity was determined by the flame structure near the flame's leading edge. Furthermore, gas phase radiation heat transfer played an important role in characterizing microgravity flame spread.

Wichman and Williams (1983) tried to develop deRis' 1969 model by adding supplied formulas for the integrated heat transfer forward of the flame in solid and gas phases. They reported that the Peclet number (which is the ratio of the thermal energy convection to the fluid to the thermal energy conduction within fluid) was small (less than unity), and that conduction played an important role in transferring heat from the solid to the gas When the Peclet number is greater that unity, the heat transfer from the gas to the solid is transferred by convection.

Downward flame spread over PMMA in an Oxygen/Nitrogen environment in normal gravity was studied experimentally, computationally and analytically by Bhattacharjee et al., (2000) they summarized that the spread rate data was presented for the first time in a thermal regime, where changes in fuel thickness from thin to thick occurred. In addition, they verified the computational model by comparing it with an analytical solution, and used the computational model to establish the transition criterion between thin and thick fuel regimes. They also concluded a simple formula for transition thickness between the thin and thick fuel regime which is:

$$\tau_{crit} = 2 \frac{\tau V_{f,Thin}}{V_{f,Thick}} \qquad (4)$$

Where;

τ_{crit} Transition criterion (mm)

τ Fuel half thickness (mm)

V_f Flame spread rate (m/s)

Downward flame spread over a thick PMMA slab was studied by Wu et al. (2003) in a mixed convection environment through experimental and unsteady numerical modeling. Their conclusion was that the freestream temperature in the opposed flow is directly proportional to the flame spread rate and inversely proportional to the velocity.

Ayani et al. (2006) studied experimental downward flame spread over PMMA sheets in quiescent air by using different thicknesses from (1.5 to 10 mm). The study showed the relationship between the thickness of the flame spread rate and the angle of the pyrolysis. From their experiments, the researchers concluded that the flame spread rate decreases with increasing thicknesses of PMMA sheets, tending to a constant value for thick samples. The angle of pyrolysis is almost constant for different thicknesses of sheets.

Chapter 3 Experimental Setup

3.1. Apparatus

A modified limiting oxygen index (LOI) as shown in Fig 3.1, also is called the minimum oxygen concentration which will support combustion, is used to measure the relative flammability of solid materials in an oxygen-enriched atmosphere. In other words, the LOI is the percent concentration of oxygen at which a small specimen will just burn downward, such as in the manner of a candle (17 for PMMA). The LOI value is related to the plastic but tells nothing about how the plastic reacts to burning in an open atmosphere. The test is considered the best-known of the standard fire tests, known as ASTM D2683, which is the standard test method for measuring the oxygen concentration of plastic (oxygen index). The flow of O_2 and N_2 inside the aluminum box spreads once it opens. The desired oxygen concentration inside the aluminum box needs some time to stability (around 3 min). Moreover, the sample starts to ignite, depends on the oxygen concentration (which could be said if O_2 concentration is high, ignition is faste).

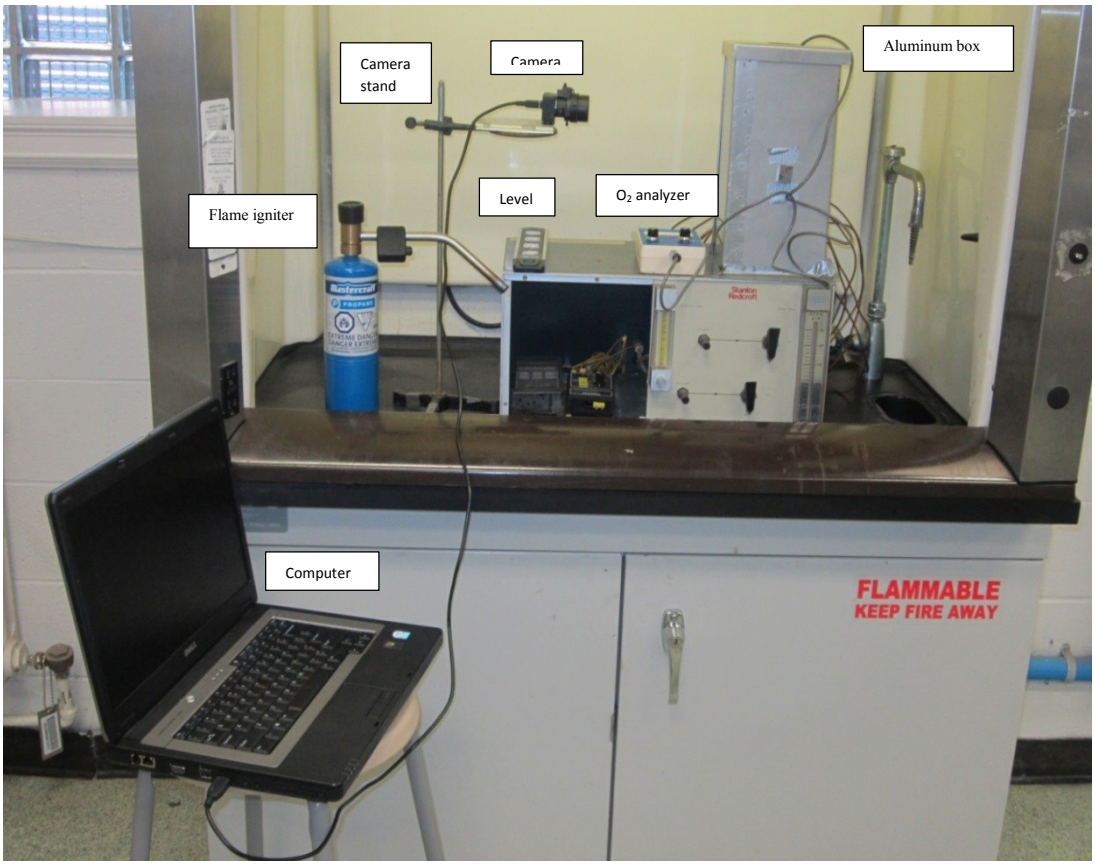

Figure 3.1 Stanton Redcroft FTA Flammability Unit

3.1.1. Test Chimney

The test chimney consists of a heat resistant glass tube that has a 100 mm inside diameter and 450 mm height. The opening at the top of the glass tube supplies an outlet around a 40 mm diameter. The bottom of the glass tube inserts to a small hole in the top of the apparatus. In the current study, the tube of glass, the chimney, was replaced because it reflected the light when images are taken by the software.

An aluminum box with a window in the front was used instead of the chimney. The window was made from anti-glare glass with dimensions, 300 mm length and 148 mm width, to prevent the reflection of the light, as shown in (Fig. 3.3). The box of aluminum was designed to use instead of the glass tube because it has the ability to resist high temperatures. The aluminum box has dimensions, 150×150×300 mm (length, width and height). The top of the box is an aluminum cover which has a circular hole with a 53 mm diameter in the middle, while the bottom of the box is open to fix in the apparatus by using tape. A special kind of paint which is RUST-OLEUM (high heat) was used to paint the inside back side of the box to prevent the reflection. Fig. 3.4 shows the use of the original chimney and how the images are unclear when it used, while Fig. 3.5 shows the aluminum box.

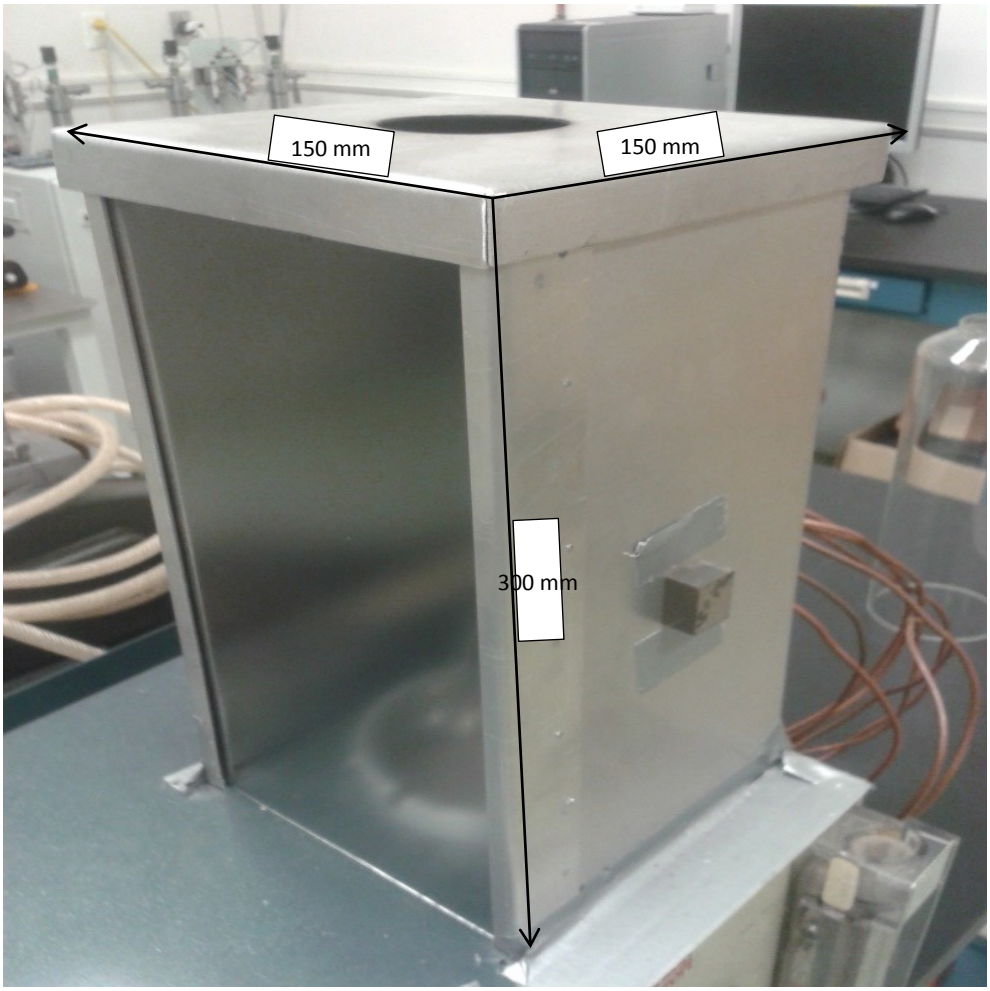

Figure 3.2 Aluminum box

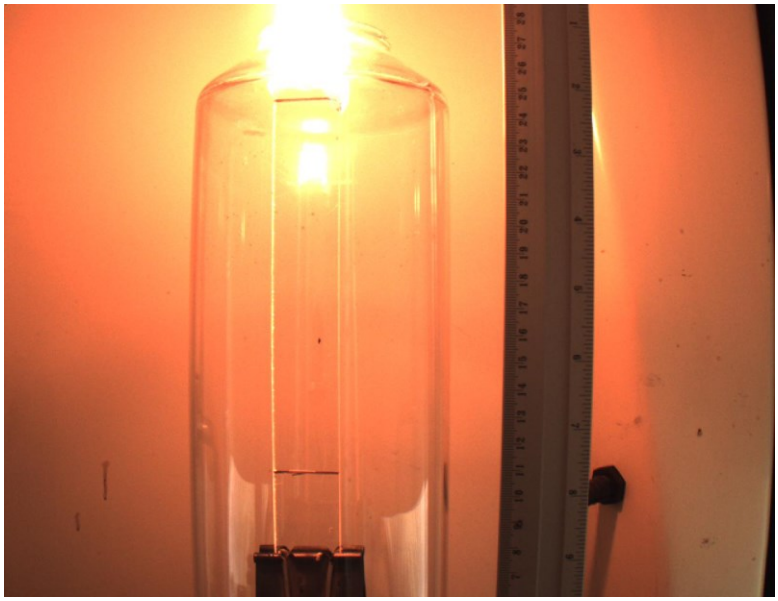

Figure 3.3 An image of the glass chimney during an experiment

.

3.1.2. Specimen Holders

A specimen holder is any small holding device, such as a paper clip, which is already inserted in the apparatus as shown in Fig 3.4. The specimen holder will support the specimen at the base and hold it vertically in center of the box

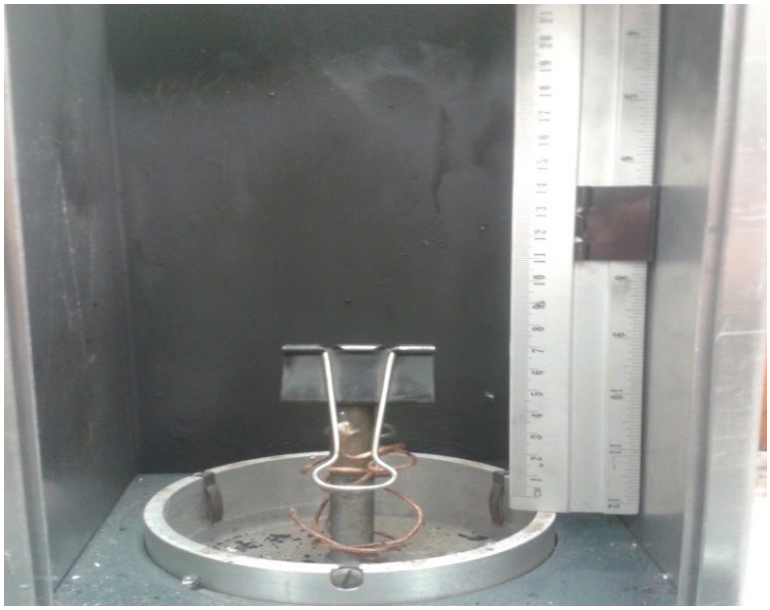

Figure 3.4 Specimen holder.

3.1.3. Gas Measurement

Gas measurement and control devices have to be suitable for measuring the concentration of oxygen and nitrogen in the gas mixture entering the box. The apparatus has two valves to control the flow rates of oxygen and the nitrogen.

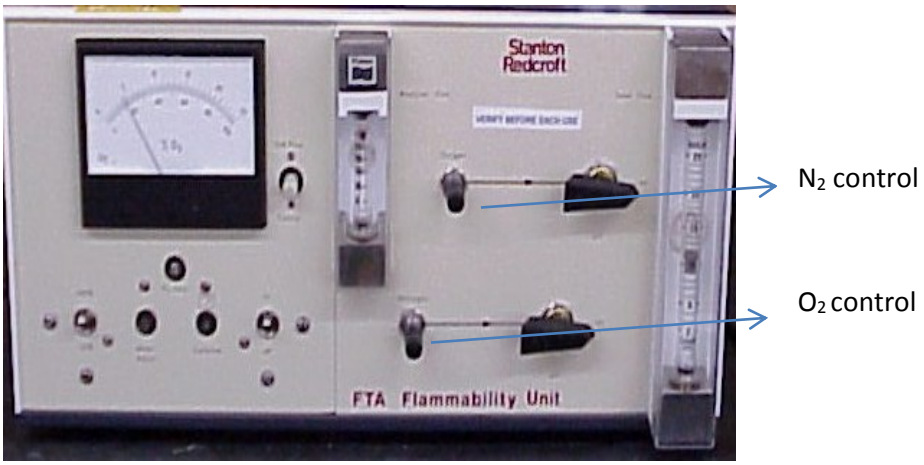

Figure 3.5 Gas Measurement

3.1.4. Flame Igniter

A propane self-igniting torch with a stainless steel burner tube was used to ignite the sample. It has a suitable diameter and can be used to ignite the sample inside the aluminum box.

Figure 3.6 Propane Self-igniting Torch.

3.1.5. Gas Supplies

Two gas cylinders of oxygen and nitrogen are needed to provide the apparatus with gas. Two cylinders are provided with pressure regulators to control the pressure gas before it enters the apparatus.

3.1.6. Oxygen Analyzer

The oxygen analyzer is used to measure the percent concentration of oxygen inside the chimney and the aluminum box. The model oxygen analyzer, with its special galvanic sensor, measures both percent concentration of oxygen in the air and parts per million of oxygen, which dissolves in aqueous solution. The range of oxygen reading would be 0-100% concentration and 0-200.0 parts per million (PPM) dissolved oxygen. The galvanic sensor must be sealed from the environment. The device needs to be calibrated before use; the calibration is done by exposing the galvanic sensor to the air once the oxygen analyzer is operated, and the oxygen percent concentration should be around 20.9% to verify the calibration. The reading of the percent concentration of oxygen must be taken as soon as it is stable; normally, it takes about 3 min to be stable.

Figure 3.7 Oxygen Analyzer.

3.2. A camera

A firefly M V 1.3 MP Color is the webcam connected to the computer in order to capture all the flame spread images. These images are analyzed to calculate the flame spread rate for flame and the angles of pyrolysis. The image capture resolution is 1328 × 1048 and with a frame rate of up to 23 fps. The webcam has a small screw to mount it onto a small base which can be fixed on a camera stand.

Figure 3.8 Firefly MV FFMV-03M2C-CS Webcam

3.3. ImageJ

ImageJ is free software which is used to analyze the image. It is a public domain Java image processing program produced by NIH (National Institutes of Health). The program could be run either as an online applet or as a downloadable application and it can display, edit, analyze, process, save and print images. Also, ImageJ has windows which contain a menu bar and toolbar. However, images, histograms, line profiles, etc. are displayed in additional windows. In addition, the measurement results are displayed in the result window. These results could be saved, copied and pasted into an Excel spread sheet. Fig. 3.9 shows a toolbar which contains tools for making selections, zooming and for scrolling images. By putting the

mouse over a tool a description is displayed in the status bar. Moreover, the program has the ability to calculate area and pixel value statistics of user defined selections, and it can measure the distance and angles. The program is available for Windows, Mac OS, Mac OS X and Linux. It is used to measure the distance which could give the velocity with known time and the angles could be measured after getting the images through this research.

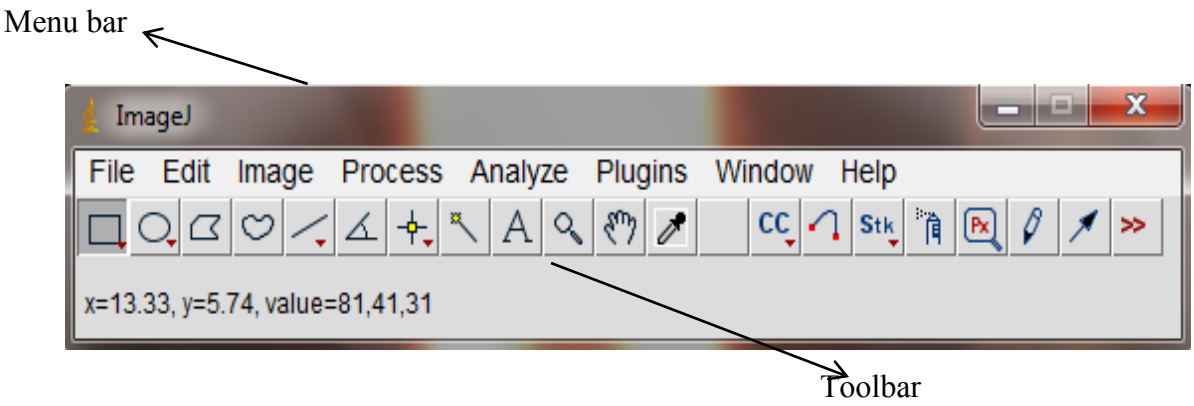

Figure 3.9 Menu bar.

Chapter 4 Experimental Method

4.1. Calibration of the Apparatus

Calibration has to be done for the apparatus, especially inside the aluminum box once the gas supplies and (N_2 and O_2) controls open. This is done by closing the nitrogen control, and opening the oxygen control. The reading must be 100% because the aluminum box was fixed by using tape. Another way to calibrate is to open the nitrogen control and close the oxygen control, then take the reading of percent concentration oxygen which has to be 0%.

4.2. Sample Preparation

The fuel samples that were used in these experiments are PMMA. PMMA was purchased from SABIC Polymershapes and then formed to different shapes and sizes at Dalhousie.

Table 4.1 PMMA with different forms and sizes

Sheets Thickness (in)	Square bars Dimensions (in)	Rods Diameters (in)
0.25 (6.35 mm)	0.5 × 0.5 (12.7 mm×12.7 mm)	0.5 (12.7 mm)
0.5 (12.7 mm)	1 × 1 (2.54 mm× 2.54 mm)	1 (2.54 mm)
0.75 (19.05 mm)		

A position mark was made on all samples before doing the experiments, which are 10 cm from the bottom of the samples. The marks were made for the following reasons.

1. To be a sign to extinguish the flame spread by closing the oxygen control and keeping the nitrogen control opens (test would take some time to extinguish).
2. The mark position helps to be a united sign for measuring the flame spread rate and angle of pyrolysis. The measurements should be stopped when the flame spread is 2 cm above the marked position because it needs enough distance to measure the velocity for all the samples and stop at the same mark.

The initial step of each experiment after preparing the sample and making the mark position is placing the fuel sample into the sample holder. Once the sample is placed into the sample holder, it needs to be adjusted using an aluminum level, which is mentioned in (3.2.8) to be straight and parallel with a ruler. A picture of the sample fixed inside the aluminum box is shown in Fig. 4.1, which was taken from a sheet sample with a 0.75 inch thickness at 20% percent concentration of oxygen.

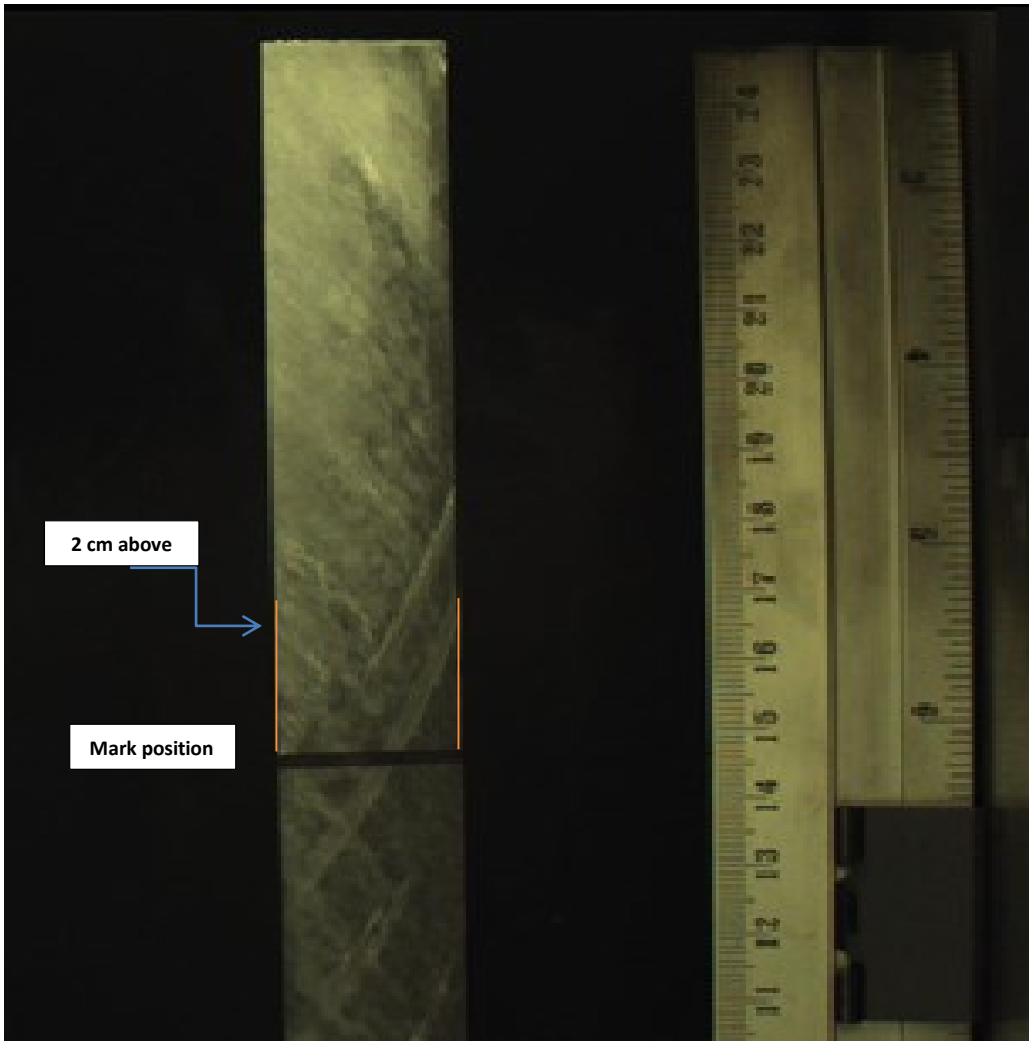

Figure 4.1 Sample set up inside the aluminum box

4.3. O_2 and N_2 Controls

After the fuel sample is ready, the gas supply valves (O_2 and N_2) on the cylinders were opened to provide the apparatus with oxygen and nitrogen. Then, the oxygen and nitrogen control device from the apparatus control panel were opened. After that, by using an oxygen analyzer, the percent concentration oxygen inside the aluminum box was measured to verify the desired percent for each experiment. The accuracy of oxygen analyzer is ±1 concentration of full scale. The concentrations of oxygen which were used for these experiments are listed in Table 4.2.

Table 4.2 Number of repetitions.

Oxygen percent %	Repetition numbers
20	-
21	3
22	-
24	-
26	3

All of the samples should burn at these percent concentrations of oxygen without repetition, except two oxygen concentrations, which are 21 and 26%. The repetition was done three times at 21 and 26% oxygen to minimize the error (the error bar and standard deviation are shows in the appendix E). The reason to do the repetition only at 21 and 26% of oxygen concentrations is because of the lack of the samples. (See appendix E)

The temperature inside and outside the aluminum box should be measured when the oxygen and nitrogen gas enter the aluminum box. The temperatures were taken by using a thermocouple, and recount to be almost the same, 21 to 22° C. Therefore, it was not considered through the experiments.

4.4. Image Analysis

Once all of the experimental steps were performed and the required oxygen concentration was verified, a camera was set on a camera stand in front of the sample, which is opposite to the aluminum box then connected to a computer. The webcam was positioned to acquire the maximum visibility of flame spread.

As mentioned above, a ruler scale was fixed inside the aluminum box next to the sample to calibrate the image (how many pixels in 1 cm) before burning each sample. Images were

acquired by using camera software (FlyCapture2 camera selection) program before igniting the sample to calibrate it by ImageJ software before each experiment, as shown in Fig. 4.2 and 4.3.

The calibration should be done before each experiment as soon as the fuel sample is fixed into the specimen holder, and it should be adjusted to be straight with the ruler by using the aluminum level. Once the calibration is performed, the time to take frames should be set to every 10 s (10000 ms) and be ready by the same camera software, which is FlyCapture2 camera selection.

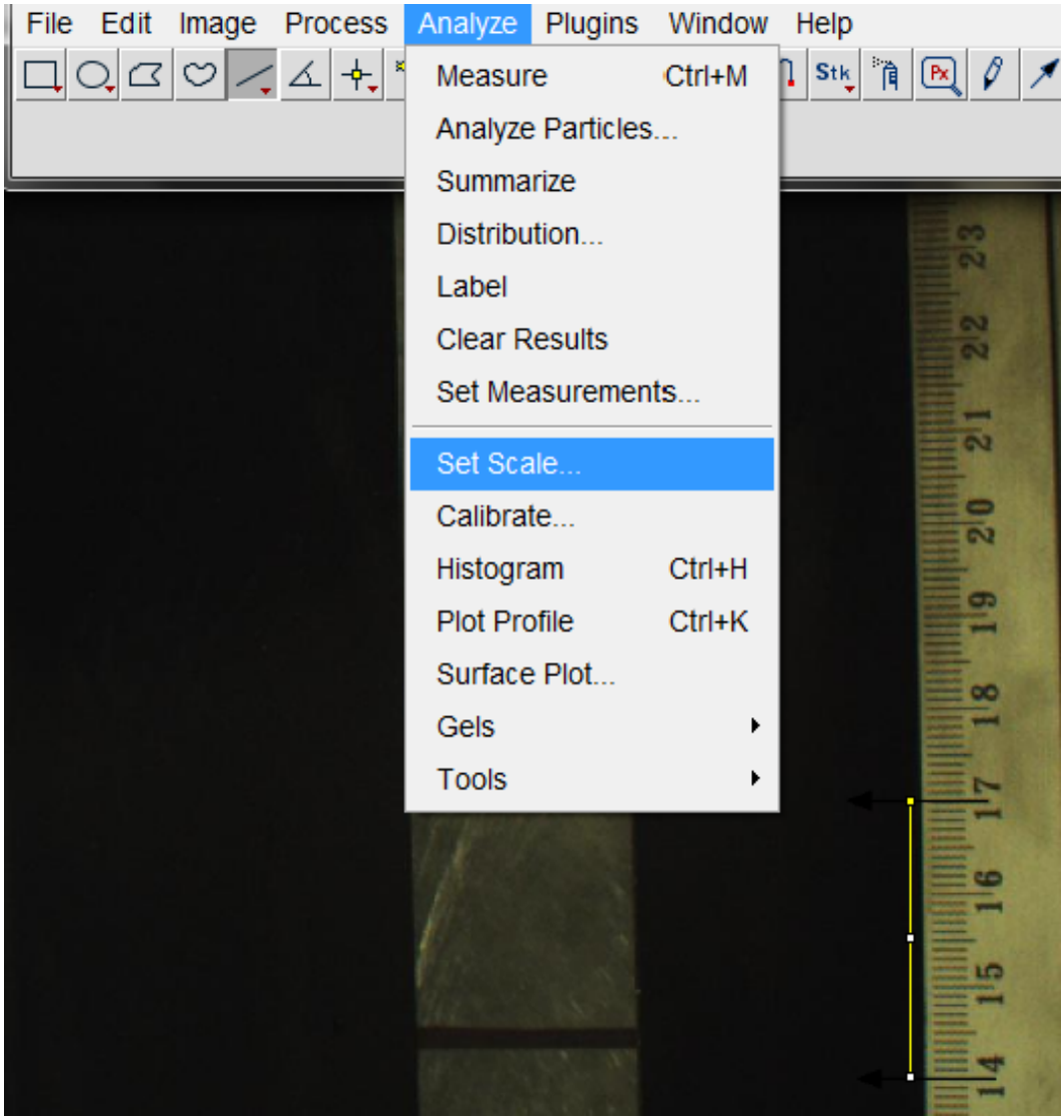

Figure 4.2 Set scale to calibrate the image.

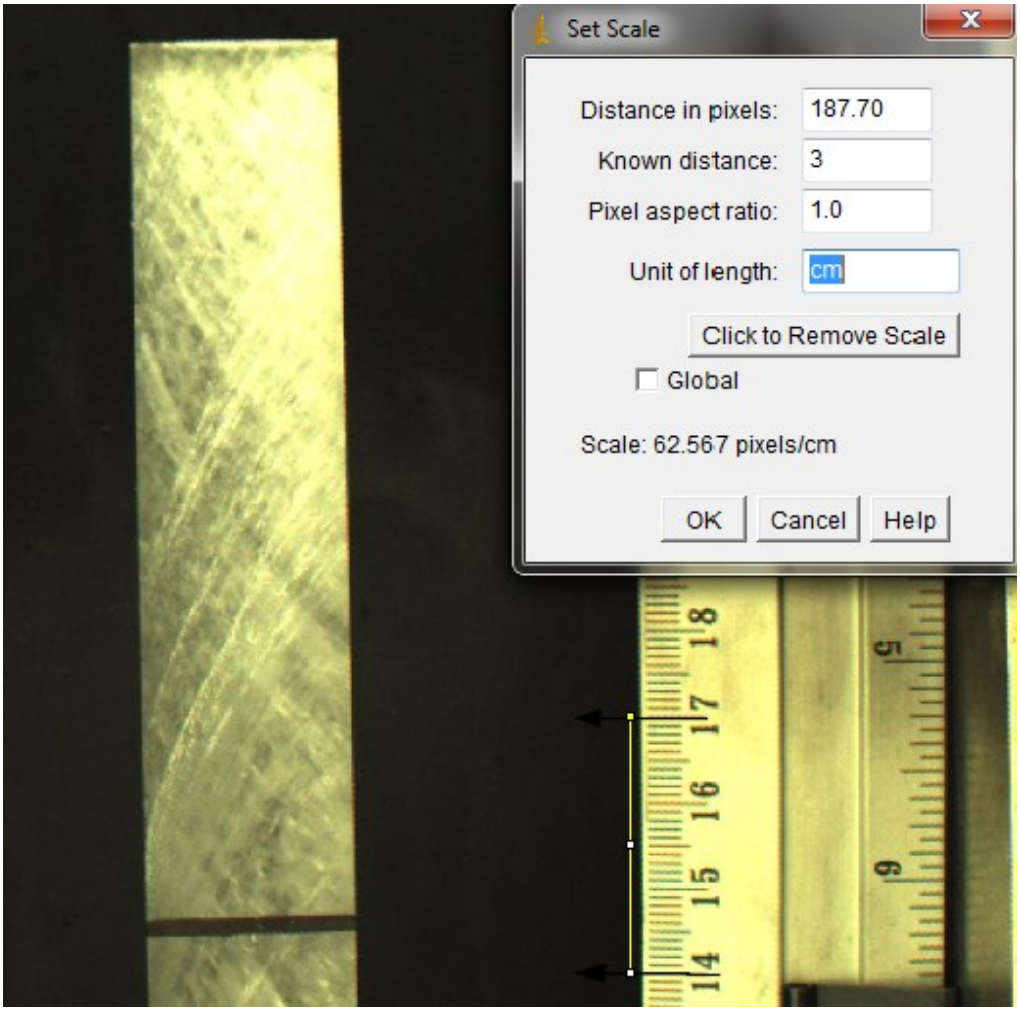

Figure 4.3 Set scale to calibrate the image for ImageJ.

A propane self-igniting torch, which was mentioned in 3.2.4, was used to ignite the sample after opening the oxygen and nitrogen from the gas supply cylinders and control valve from the apparatus control panel to verify the desirable percent of oxygen concentration. When the sample started to ignite, the camera was set to start to take frames for flame spread at the same time, every 10 s, using the camera software that is shown in Fig. 4.4 below.

The camera would continue to take frames until the flame reaches the mark position, which is made on the fuel samples. Subsequently, the camera would be stopped, either by setting a reasonable time to stop or by stopping it manually. Also, the flame has to be extinguished by closing the oxygen control while keeping the nitrogen control open when it reached the marked position.

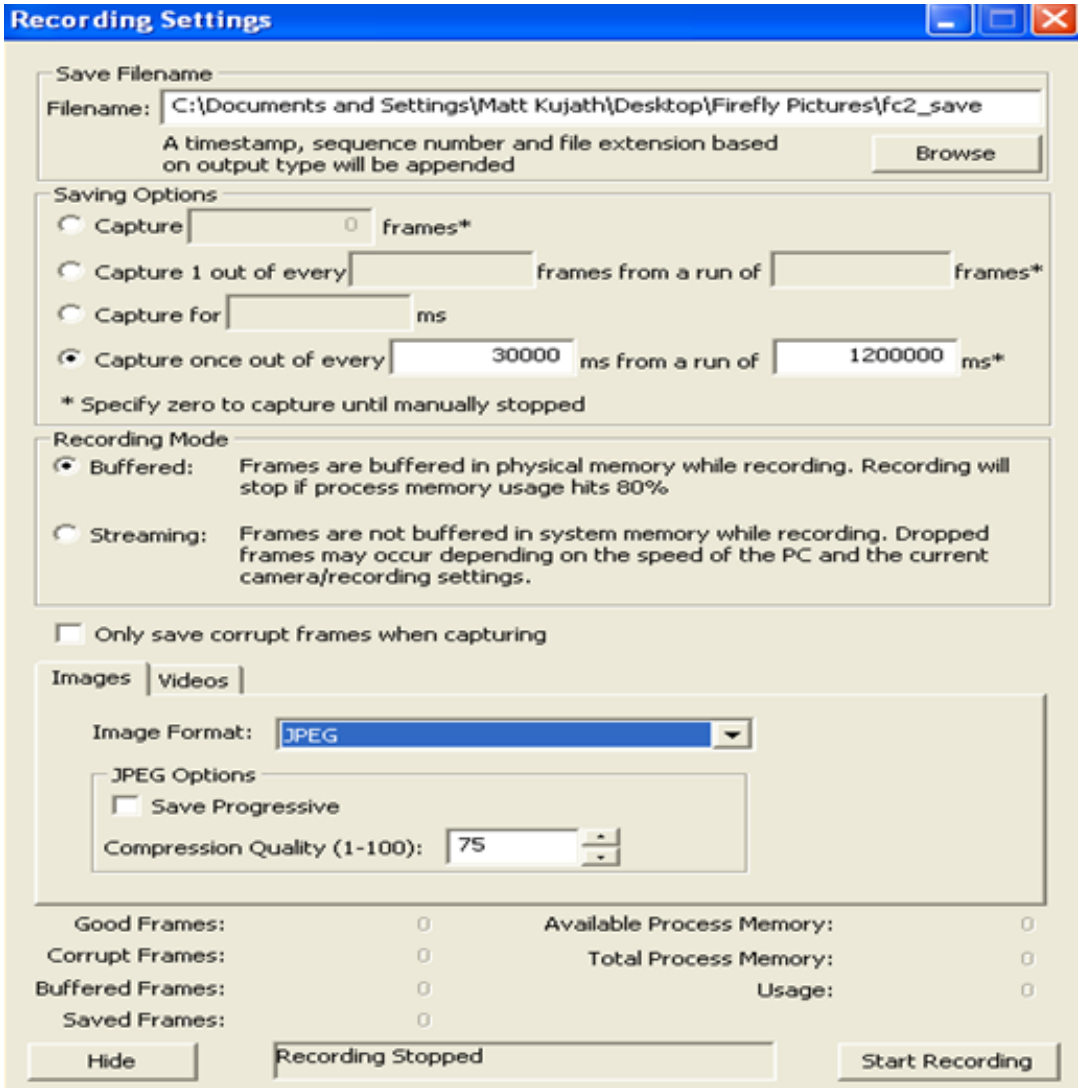

Figure 4.4. Camera recording settings.

Many frames were obtained for flame spreading for each test for the different shapes of fuel samples and different percent concentrations of oxygen. These frames then needed to be analyzed to measure the flame spreading rate and the angle of pyrolysis. The next step is to measure the distance from the left and right edges and the mid-point of flame spread on the fuel sample to the marked position each 10 s from the camera shot while knowing the time. The flame spread rate (cm/s) was calculated by dividing the distance over the difference between the total time (which is the time from ignition until the flame reaches the marked position on the fuel sample) and the burning time (the time on which the image was taken) for each image. However, the relationship will be represented in the results between the average

of flame spread rate at three points (cm/s) and the burning time at each oxygen concentration percent. As we mentioned above, the flame spread rate should be calculated at three points on the fuel sample, which are the edges (left and right edge) and the middle of fuel sample where the angle of pyrolysis appears as shown in Fig. 4.5 below. The velocities were mentioned above, were measured at the glass transition line as shown in Fig 4.5.

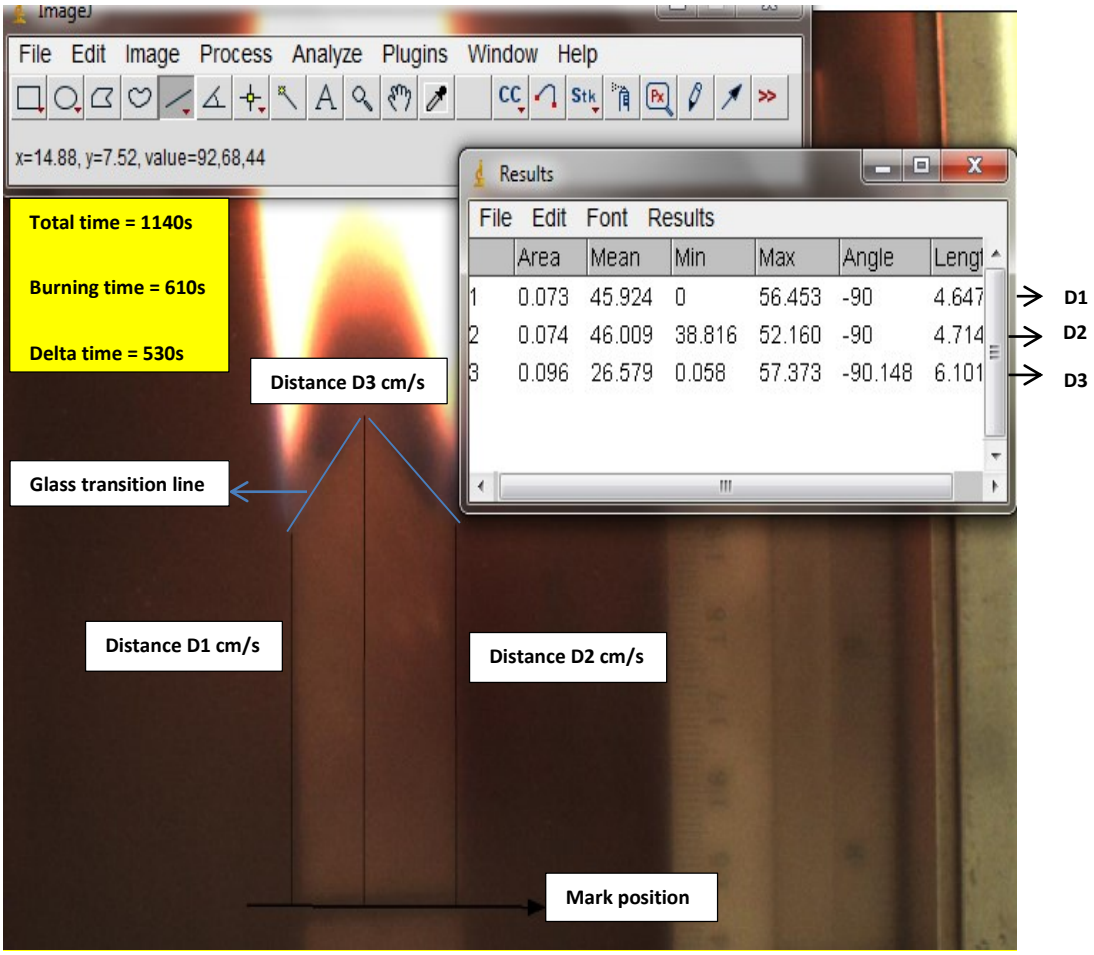

Figure 4.5 Picture showing three flame spread points on the sample.

The frame above was taken from a sheet sample with a 0.75 inch thickness at 20% percent concentration of oxygen. The image above is number 60 out of 113 images of burning sample. The time which is consumed until image number 60 is 610 s (burning time) out of 1140 s (total time for 113 images) for burning the sample until the marked position. Each distance (distance 1, 2 and 3) from the distances above should be divided over the change in time, which is the difference between the total and burning time to get the flame spread rate. The

error should be considered when the points determine for measuring the distances on the sample after the burning as shown in fig 4.6 which is ±0.07.

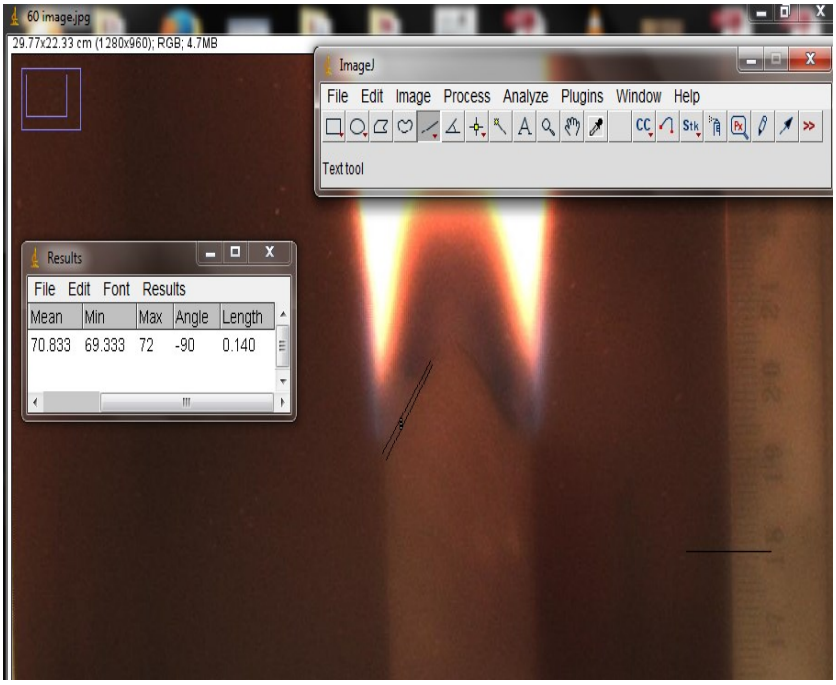

Figure 4.6 The error when determine the position for measuring the distance

The average flame spread rate as we mentioned above would be the average of the flame spread at each point. The small window in Fig. 4.5 above shows the measurement of distances (D1, D2 and D3). Those measurements were exported two an Excel spreadsheet to simplify the calculation.

These steps were done for all images at each percent concentration of oxygen in addition to different shapes of fuel samples to calculate the flame spread rate (cm/s). An example is shown in the appendix A of how the flame spread rate calculations were done.

Once the flame spread rate was measured, the angle of pyrolysis, which shows through the transition line, was calculated for each image of the sample burning images as shown in fig 4.6; then, the average was calculated. The ImageJ program could measure the angle from the sample burning images by choosing the angle option from the ImageJ toolbar. These steps should be performed for each percent concentration of oxygen and different shapes of fuel samples (sheets and square bar), but rod samples have a mathematical method after burning that will be explained in the results chapter to calculate the angle of pyrolysis.

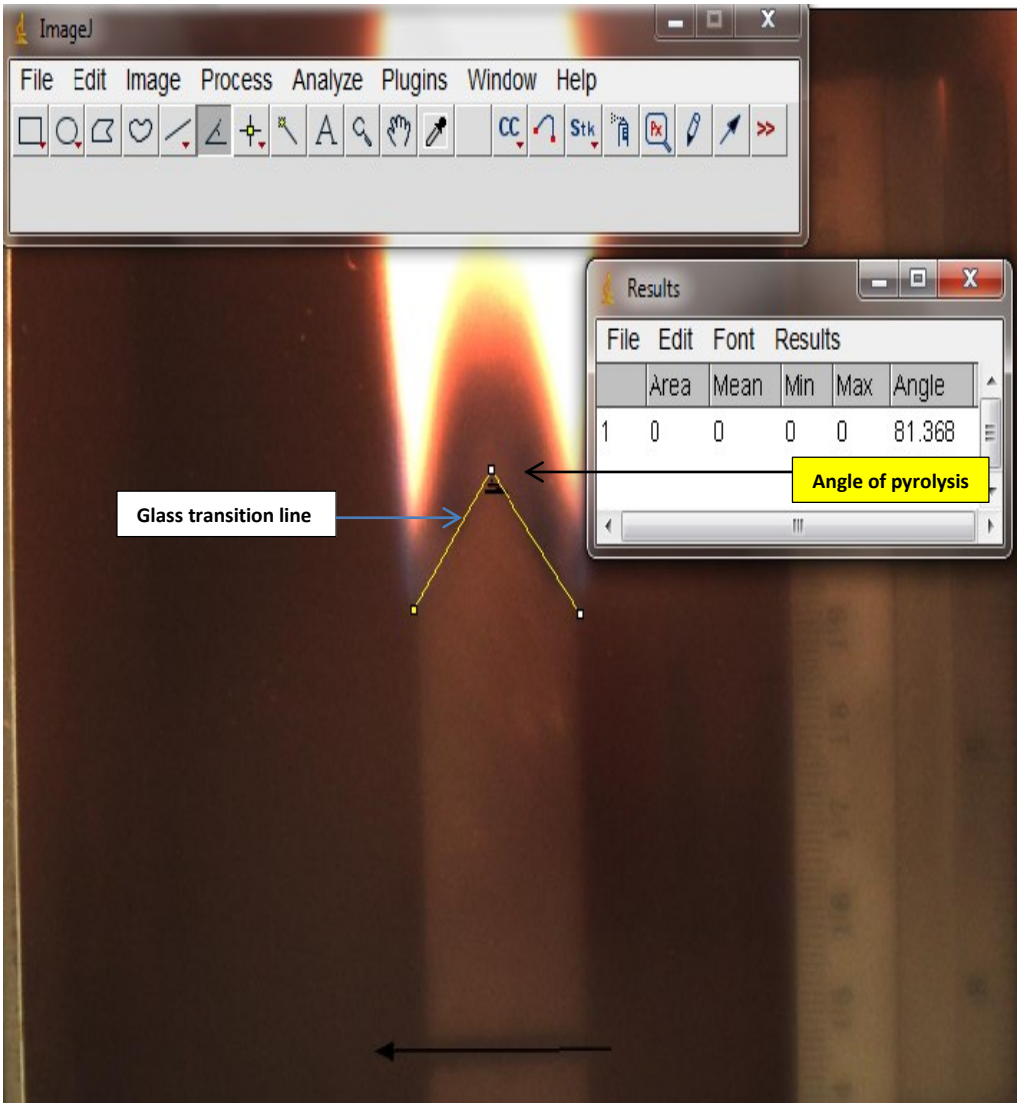

Figure 4.7 Angle of pyrolysis measurements.

Fig. 4.7 shows, different images (85, 90, 95, 100, 105 and 110) for the angle of pyrolysis at different burning times (1056, 1071, 1086, 1101, 1116 and 1113 s) for the same sample which was mentioned above.

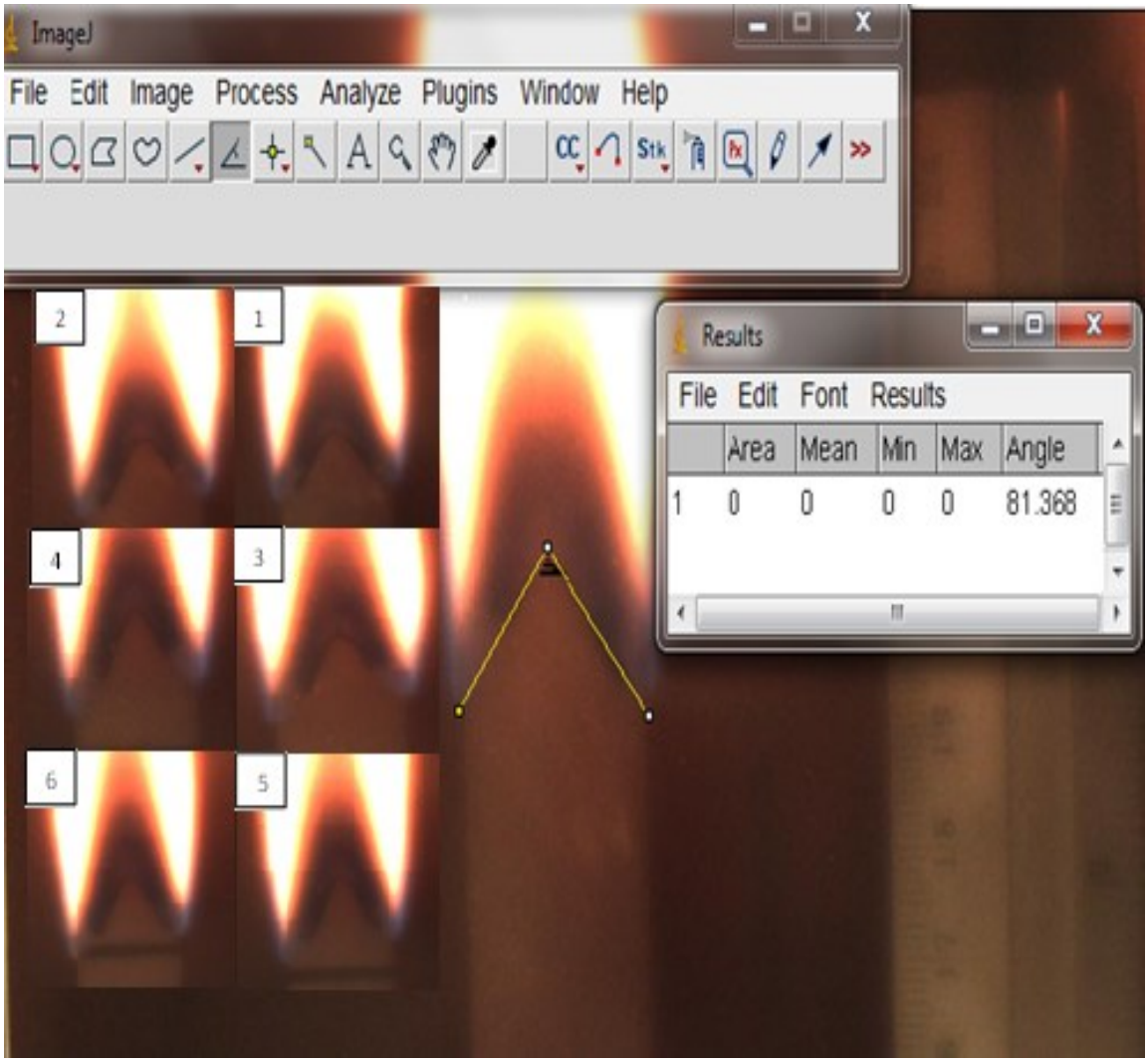

Figure 4.8 Different angles of pyrolysis measurements.

4.5. The Calculation of the Angle of Pyrolysis on Rod of PMMA

The angle of pyrolysis was not clear enough when rods of PMMA were burned. Therefore, the software which was used to measure the angle of pyrolysis for other shapes (sheets and square) was useless to measure the angle of pyrolysis on rods with different diameters. However, some calculations have been done to measure the angle of pyrolysis by using an electronic caliper with a digital display. Two points were determined on the rod with taking the vertical distance between them, which is (h). Then, the diameters (d_1 and d_2) have to be calculated at these points on rods by using an electronic caliper. The radius of two diameters

was taken, and a triangle which contains a right angle would appear, because one of the diameters would be bigger than the other. The angle could then be calculated as shown in Fig. 4.10 below

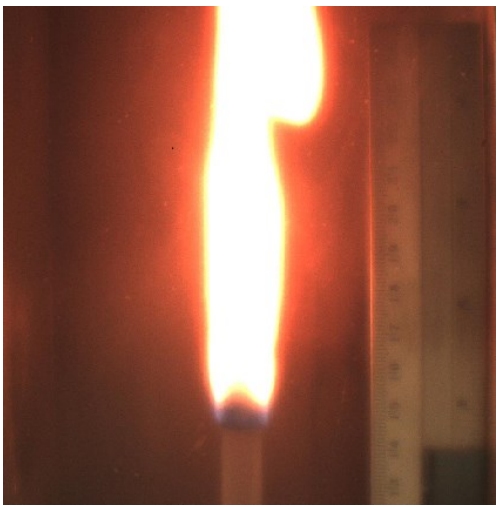

Figure 4.9 Image of flame on PMMA rod 0.5 in diameter.

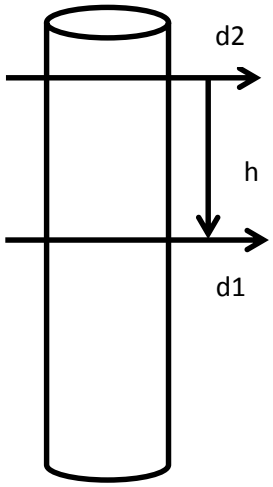

Figure 4.10 The measurements on the PMMA rod with 0.5 in diameter.

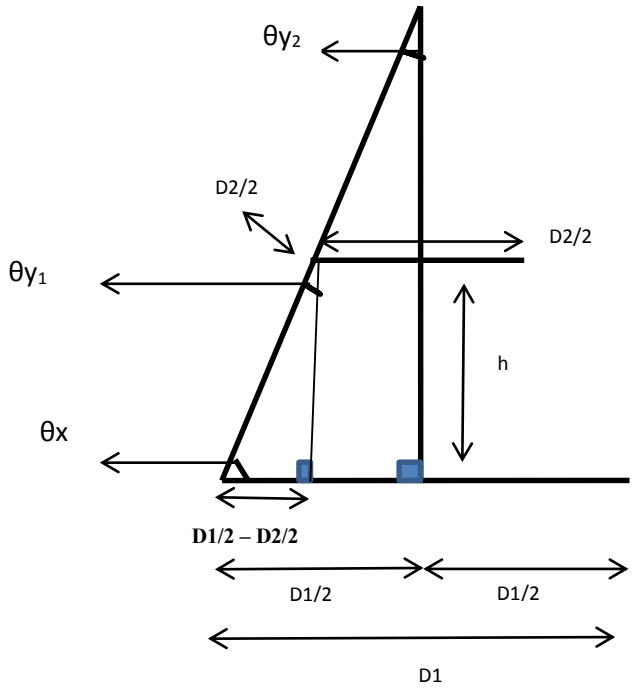

Figure 4.11 Triangle with the measurements and the angles.

After using an electronic caliper with a digital display to measure the diameters for rods with 0.5 and 1 in and measuring the distance between them at different oxygen concentrations. However, the values of θ_x and θ_y could be found by substituting the following equations:

$$\Theta_x = \tan x^{-1} \left(\frac{H}{\frac{D1}{2} - \frac{D2}{2}} \right) \qquad (4.1)$$

The total of the triangle angles is 180°. Since the triangle has a right angle (90°), θ_{y2} could be calculated from:

$\theta_{y1} = 180 - 90 - \Theta_x$ (4.2) $\theta_{y1} = \theta_{y2}$

θ_{y2} is known as a half of the angle of pyrolysis; therefore, it has to be multiplied by 2.

Table 4.3 The results after the substitution in equations (4.1) and (4.2).

Different oxygen concentrations %	The angle of pyrolysis for rod with 0.5in diameters (Deg.)	The angle of pyrolysis for rod with 1 in diameters (Deg.)
20	32.3	26.9
21	18.4	13.4
22	15.1	17.5
24	10.6	10.5
26	8	8.9

Another way was used to confirm these calculations, which is cutting a cylinder section from the rod sample with 1 inch diameter burned at 26% (second repeat which was 8.7°) of O_2 where the transition line appears as shown in Fig 4.11:

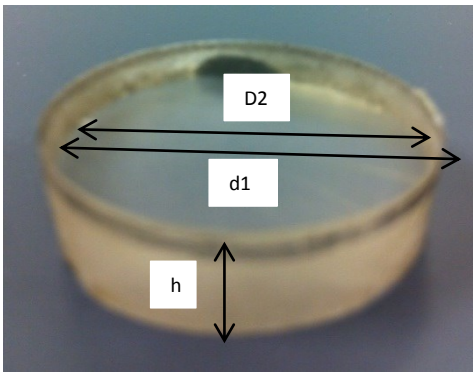

Figure 4.12 Cylinder section from 1 in diameter rod sample

By measuring the top and bottom diameters (d_1 and d_2) and the side length (h) on this section as shown in fig 4.11

Where:

d_1 = 23 mm , d_2 = 22 mm and h = 7 mm

Applying the triangle which is shown in fig 4.10 and after substituting in equations (4.1 and 4.2)

Θ_x= 85.9° and $\theta_{y2} = \theta_{y1}$= 4.1° where

The angle of pyrolysis = 2* θ_{y1} = 2 * 4.1 = 8.2°

Chapter 5 Results and Discussions

5.1. Effect of Ambient Oxygen Concentrations on Flame Spread Rate for Sheets

5.1.1. Effect of Ambient Oxygen Concentration% on Flame Spread Rate (cm/s) for Fuel Sheets with 0.25 in Thickness

The effect of oxygen concentration on flame spread rate (velocity) using different concentrations of oxygen, which were (20, 21, 22, 24 and 26%), was studied. Fuel sheets of PMMA with 0.25-in thickness were burned until a marked position, which was made on all of the used samples, at different oxygen concentrations. As mentioned in chapter 4, the measurements of flame spread rate and the angle of pyrolysis appeared when the transition line appears after burning the materials. Fig. 5.1 shows the experimental results of flame spread rate versus oxygen concentrations. The flame spread rate increases as the oxygen concentration increases. The flame spread rate goes up quickly at high concentrations of oxygen (24 and 26%). On the other hand, the flame spread rate rises slowly at other concentrations (20, 21, and 22%). The trend has been changed between 22% and 24% of oxygen concentration regard to some reasons that are concluded: mixing of O_2 and N_2 flow inside the aluminum box increases the oxygen concentration at the top of aluminum box (beside the flame on the sample) if the desired oxygen concentration at the bottom of aluminum box less than 21% while it decreases the oxygen concentration beside the flame on the sample (at the top of aluminum box) if the oxygen concentration at the bottom of aluminum box more than 21%, the heat rate also increases as oxygen concentration increases which cause to rapid flame spread, the accuracy and the stability of the oxygen analyzer to verify the desired the percentage of oxygen concentration, the diffusion inside the aluminum box increases with increasing the concentration of oxygen and also because of the difference between PMMA shapes are used. Those reasons are common in some cases through the results. It could be concluded that there is a direct relationship between the flame spread rate and ambient oxygen concentrations.

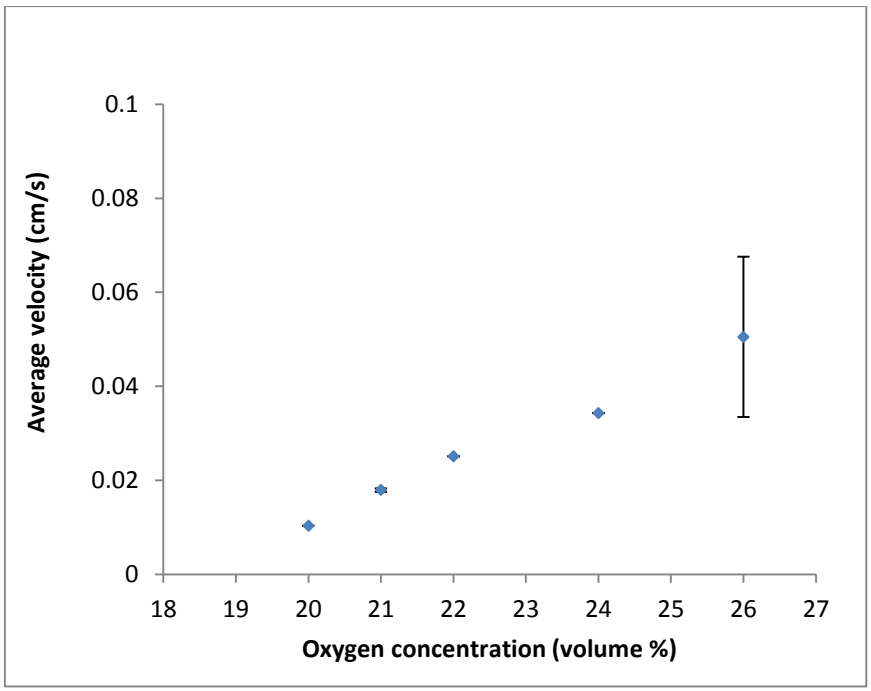

Figure 5.1 Flame spread rate versus the oxygen concentrations for 0.25 in sheet thickness.

5.1.2. Effect of Ambient Oxygen Concentration on Flame Spread Rate (cm/s) for 0.50in Thickness Fuel Sheets

Sheets of PMMA were also cut with 0.50-in thickness and burned at the same oxygen concentrations, which are (20, 21, 22, 24 and 26). A direct relationship was produced in fig 5.2 between the flame spread rate and different oxygen concentrations where the flame spread rate peaks with a high concentration of oxygen while it grows with 20, 21 and 22% oxygen concentrations. The trend changed at 21% and 22% of oxygen concentration because of the previous reasons: flow mixing and sample shape in addition to 21 and 22% of oxygen concentration it is close to the atmosphere percentage of oxygen which is almost 21%. The trend line changed little bit from 21 to 22% of oxygen concentration in this case, the reasons for that are, 21% of oxygen concentrations were repeated three times at which could minimize the error and makes the average of velocity more accurate while 22% of oxygen concentration was done once because of the lack of samples. Also, the increasing of the mixing of O_2 and N_2 flow inside the aluminum box is a reason to increase the oxygen concentration. In addition to, the other reasons that were mentioned in 5.1.1.

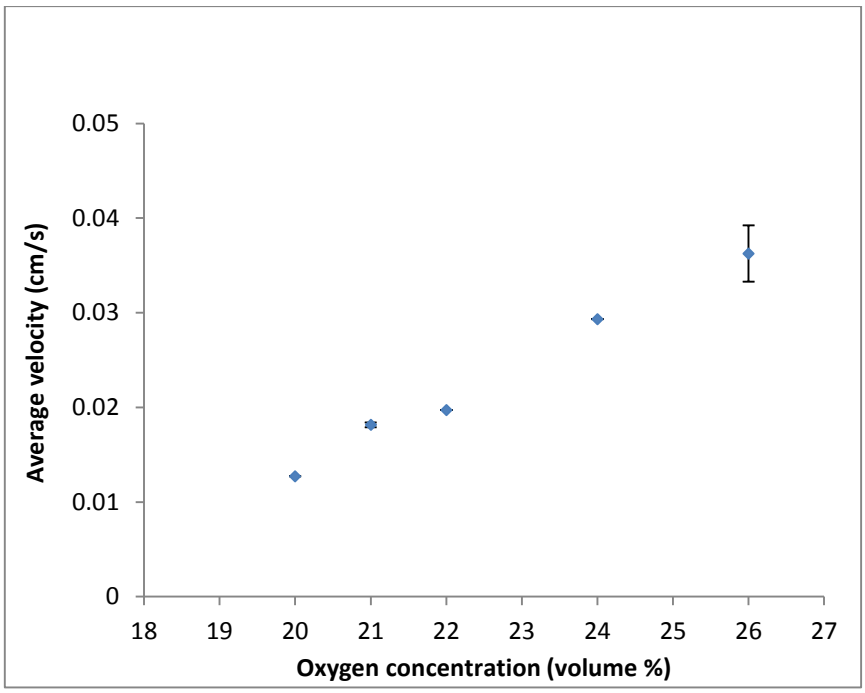

Figure 5.2 Flame spread rate versus the oxygen concentrations for 0.50 in sheet thickness.

5.1.3. Effect of Ambient Oxygen Concentration% on Flame Spread Rate (cm/s) for 0.75in Thickness Fuel Sheets

Fig. 5.3 shows that the flame spread rate increases with the increase in oxygen concentration, even when using sheets of PMMA with 0.75-in thicknesses as fuel to burn. However, the same relationship with sheets with 0.25 and 0.50-in thickness would occur, which is the flame spread rate grows with 20, 21 and 22% oxygen concentration, but it surges at 24 and 26% of oxygen concentration. It could be seen that the flame spread rate is directly proportional to the oxygen concentration.

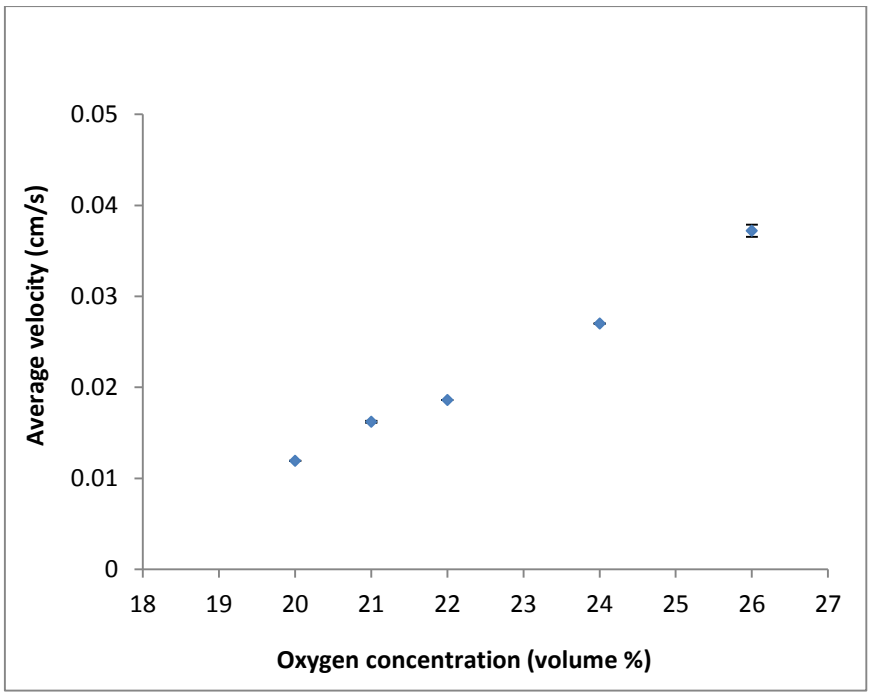

Figure 5.3 Flame spread rate versus the oxygen concentrations for 0.75 in sheet thickness.

5.1.4. The Comparison between An oxygen Concentrations and Flame Spread Rate for Different Thicknesses (0.25, 0.50 and 0.75 in)

The comparison between flame spread rate and oxygen concentrations for sheets with different thicknesses (0.25, 0.5 and 0.75-in) is shown in Fig. 5.4. The samples which have thinner thicknesses would burn faster than those that are thicker, especially when the oxygen concentrations are more than 21%. However, the flame spread rate goes up quickly at high concentrations of oxygen. In other words, there is a direct relationship between the flame spread rate and the oxygen concentrations. In addition, the flame spread rate decreases with increasing thicknesses of PMMA sheets, which totally agree with Ayani's conclusion that "Flame spread rate is inversely proportional to the sheet thickness". The measurements of flame spread rate at different oxygen concentrations was repeated not more than three times because of a lack of PMMA sheet material to minimize the error and confirm them at 21 and 26%. The average of these repetitions at each oxygen concentration was used in Fig. 5.4. (The results are shown in appendix B.1 to B.3)

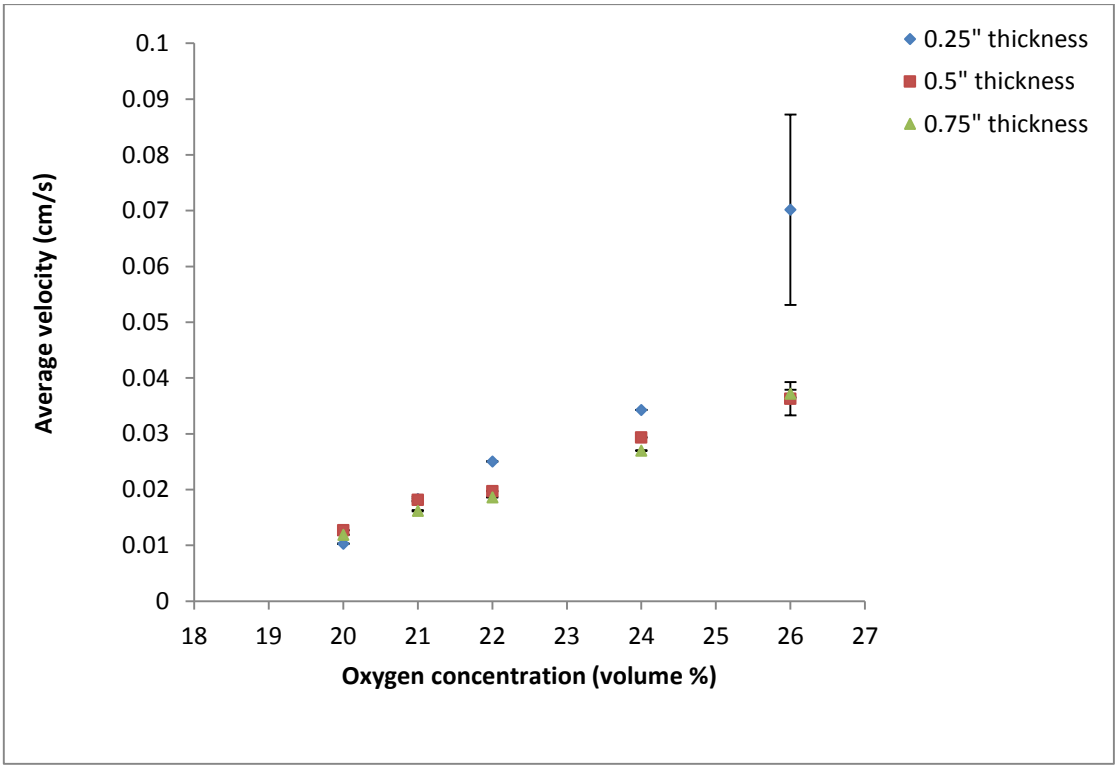

Figure 5.4 Flame spread rate versus Oxygen concentrations for sheets with different thickness.

5.2. Effect of Ambient Oxygen Concentrations on Angle of Pyrolysis for Sheets.

5.2.1. Effect of Ambient Oxygen Concentration% on Angle of Pyrolysis for Fuel Sheets with 0.25in Thickness

The relation between the angle of pyrolysis and oxygen concentration is shown in Fig. 5.5 below. The angle of pyrolysis reaches to the highest value at the smallest oxygen concentration, which is 70.2° at 20% then it declines to 62.9° at 21% of oxygen concentration. However, the angle of pyrolysis drops to 48, 47.3 and 45.1 at 22, 24 and 26% oxygen concentrations, respectively which is more than O_2 in atmospheric, which makes the sample burning faster that 21 and 20% of oxygen concentrations. However, The angle is almost constant at high concentrations. In other words, the angle of pyrolysis is inversely proportional to some of the oxygen concentrations where it decreases as oxygen concentrations decrease.

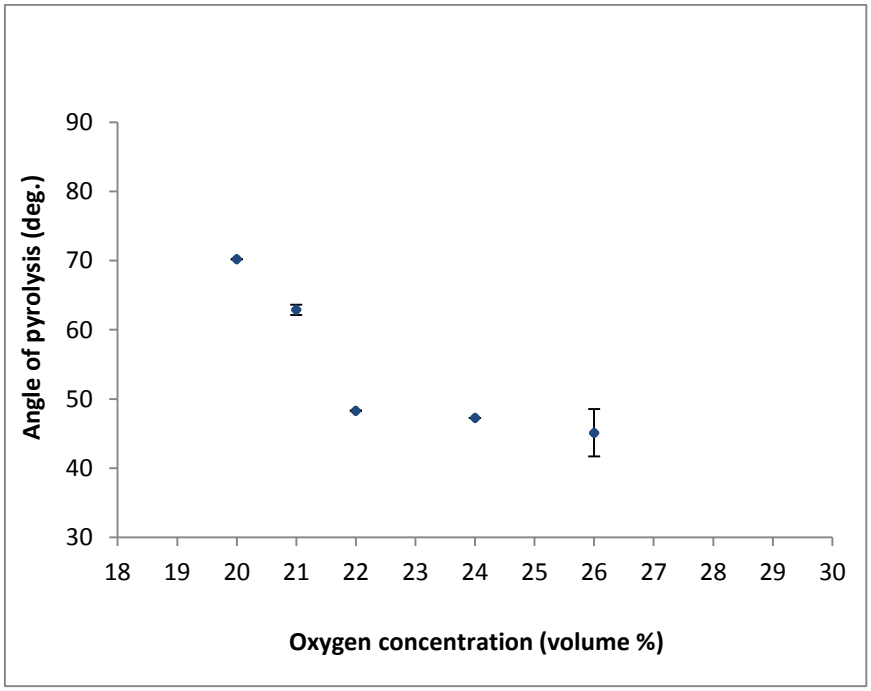

Figure 5.5 Angle of Pyrolysis versus the oxygen concentrations for 0.25 in sheet thickness.

5.2.2. Effect of Ambient Oxygen Concentration% on Angle of Pyrolysis for Fuel Sheets with 0.50 in Thickness:

Fig. 5.6 shows an inverse relationship between the angle of pyrolysis and oxygen concentrations. At 20% oxygen concentration, the angle of pyrolysis was at the highest value which is 71.6° and then starts to decrease slowly at 21 and 22% of oxygen concentrations to reach 60.7 and 58.1° respectively. The angle of pyrolysis drops as oxygen concentration increasing until 44.3° at 24% of oxygen concentration and it changes a little bit at 26% of oxygen concentration to be 42.6°.

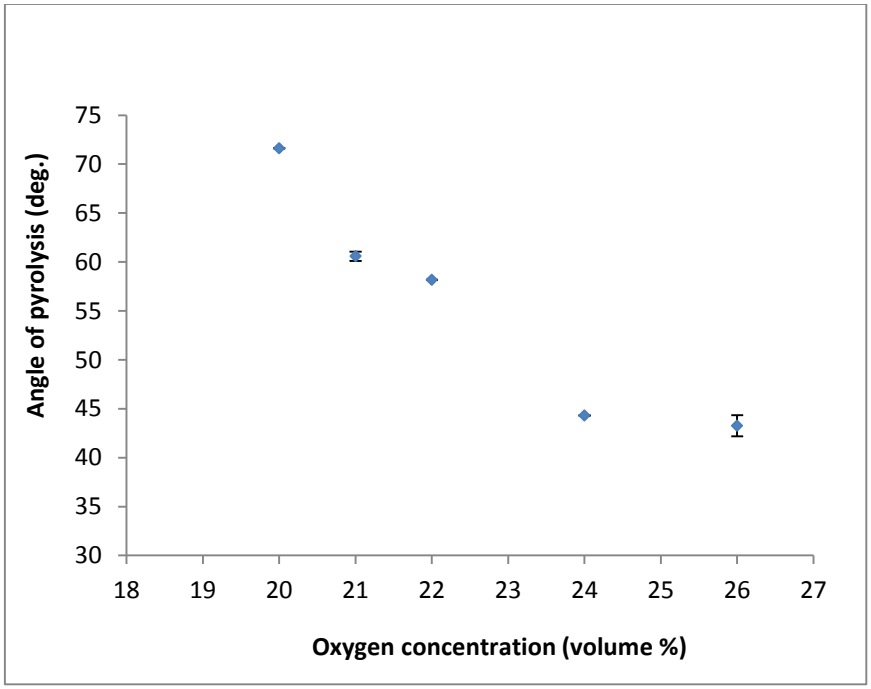

Figure 5.6 Angle of Pyrolysis versus the oxygen concentrations for 0.50 in sheet thickness.

5.2.3. Effect of Ambient Oxygen Concentration% on Angle of Pyrolysis for Fuel Sheets with 0.75 in Thickness:

The effect of oxygen concentration on the angle of pyrolysis for sheets with 0.75 in thickness is the same as with sheets with 0.25 and 0.50 in thickness, but the samples with 0.75 in thickness need much time to burn, and as a result they would make more images to analyze for measuring the angle of pyrolysis. This can be seen in Fig. 5.7, as the angle of pyrolysis decreases as the oxygen of concentrations increases, which concludes that there is an inverse relationship between the angle of pyrolysis and oxygen concentration.

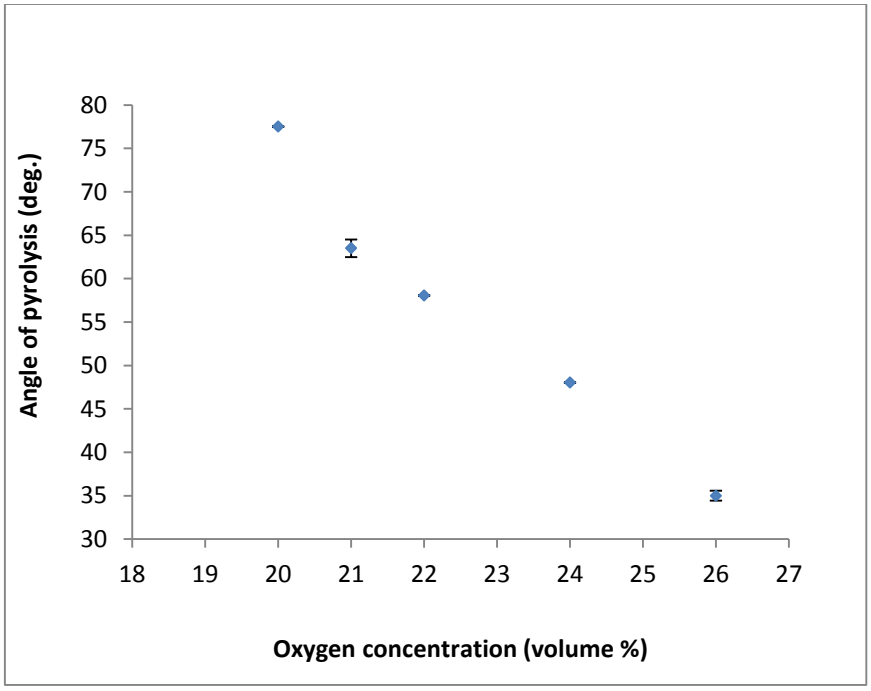

Figure 5.7 Angle of versus the oxygen concentrations for 0.75 in sheet thickness.

5.2.4. The Comparison between An oxygen Concentrations and the Angle of Pyrolysis for Different Thicknesses (0.25, 0.50 and 0.75 in):

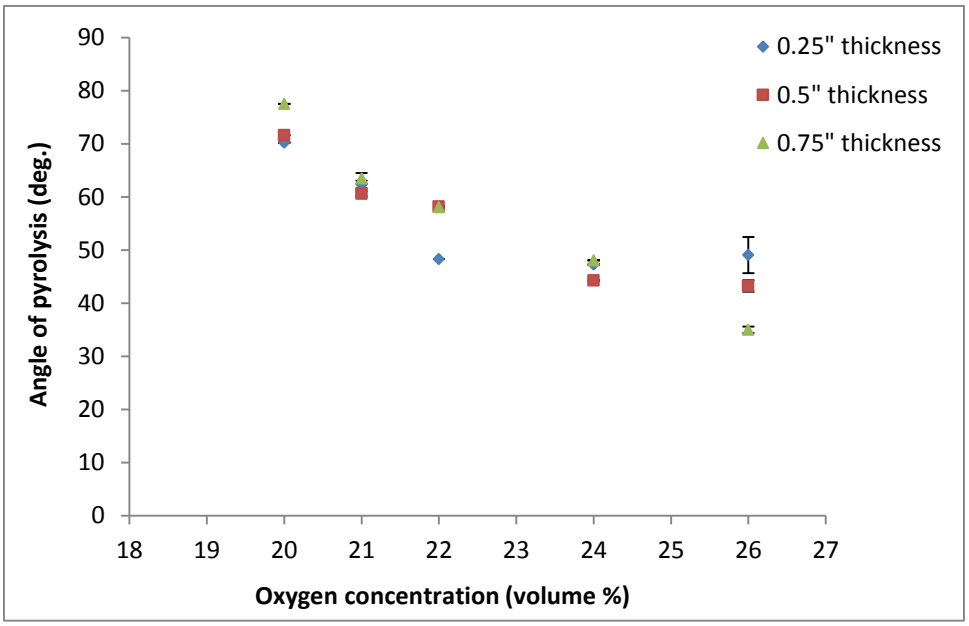

Figure 5.8 Angle of pyrolysis versus Oxygen concentrations for sheets with different thickness.

The comparison between the angle of pyrolysis and oxygen concentrations for sheets with different thickness (0.25, 0.5 and 0.75 in) shows that the angle of pyrolysis decreases with an increase in the oxygen concentration as in fig 5.8. In sheets with 0.25 in thickness, the decline of the angle of pyrolysis is (48.3, 47.3 and 45.1°) at high concentrations of oxygen (22, 24 and 26%) respectively. While the angle of pyrolysis for sheets with 0.5 and 0.75 in thickness at the same concentrations of oxygen (22, 24 and 26%), respectively, is almost the same. This validates the previous conclusion that there is "an inverse relationship between the angle of pyrolysis and oxygen concentrations". In addition, the angle of pyrolysis decreases when the oxygen of concentration increases from 20 to 21%. It can be concluded that the angle of pyrolysis does not change too much for different sheet thicknesses at the same oxygen concentration, which almost agrees with Ayani et al (2006) conclusion whereas; at different oxygen concentrations each sheet's thickness has a different angle of pyrolysis. (The results are shown in appendix B.1 to B.3)

5.3. Effect of Ambient Oxygen Concentrations on Flame Spread Rate for Different Square Rod Dimensions

5.3.1. Effect of Ambient Oxygen Concentrations on Flame Spread Rate for Square Rod with 0.5×0.5 inch Dimensions

A square section material with 0.5×0.5 inch dimensions was made from (polymethylmethacrylate) PMMA and used as fuel to burn until the marked position. The flame spread rate was almost the same (0.0164 and 0.0165 cm/s) at 20 and 21% of oxygen concentration, respectively. Then, it starts to increase with increasing oxygen concentration until it reaches a high value with a high oxygen concentration to be (0.0209, 0.0206 and 0.0393 cm/s) at (22, 24 and 26%), respectively. In fig. 5.9 it can be seen that there is a direct relationship between flame spread rate and oxygen concentration, which agrees with the relationship between the flame spread rate and oxygen concentrations when the material was sheets with different thicknesses.

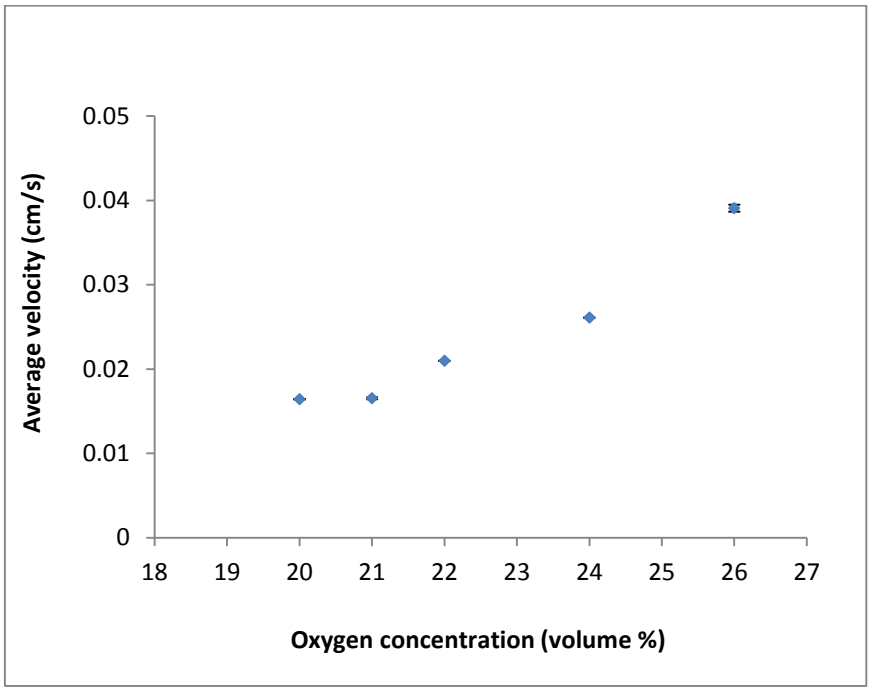

Figure 5.9 Flame spread rate versus the oxygen concentrations for 0.5×0.5 in square rod.

5.3.2. Effect of Ambient Oxygen Concentrations on Flame Spread Rate for A square Rod with 1×1 inch Dimensions

Fig. 5.10 shows the rate at which a square rod with 1×1 inch dimensions of PMMA burns at different oxygen concentrations. The flame spread rate can be calculated by measuring the distance every 30 s; then, the average of the velocities would be calculated to be a flame spread rate. Those measurements would be done for different oxygen concentrations to get a different flame spread rate as shown in Fig. 5.10. The flame spread rate at 20% oxygen concentration was the smallest value, which is 0.0155 cm/s, then starts to increase to be almost the same (0.0182 and 0.0185) at 21 and 22% of oxygen concentration. At a high concentration such as 24 or 26% of oxygen, the flame spread rate peaks (increases) with increasing oxygen concentrations.

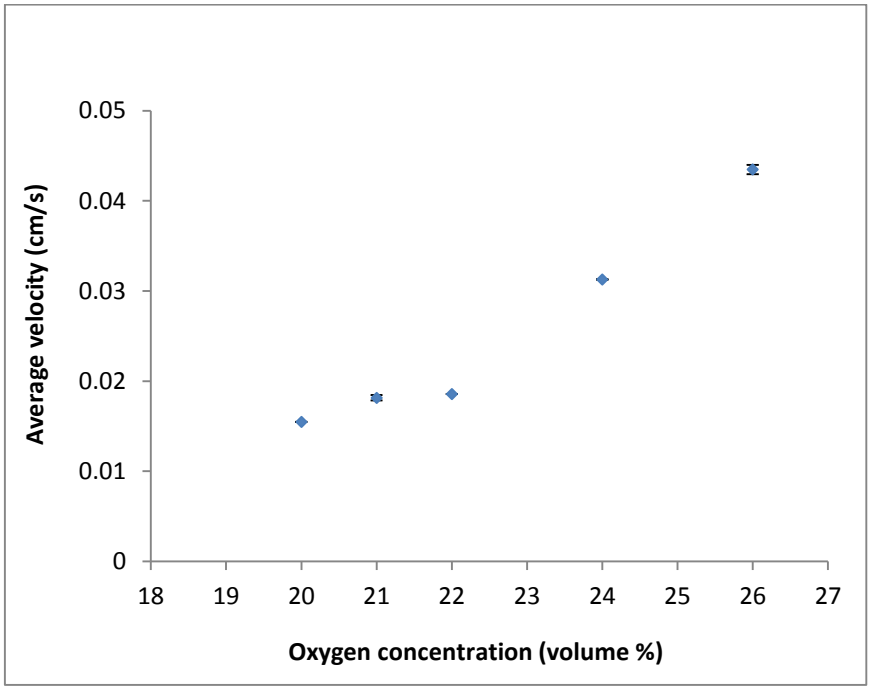

Figure 5.10 Flame spread rate versus the oxygen concentrations for 1×1 in square rod.

5.3.3. The Comparison between An oxygen Concentrations and Flame Spread Rate for Different Square Rod Dimensions (0.5×0.5 and 1×1 inch)

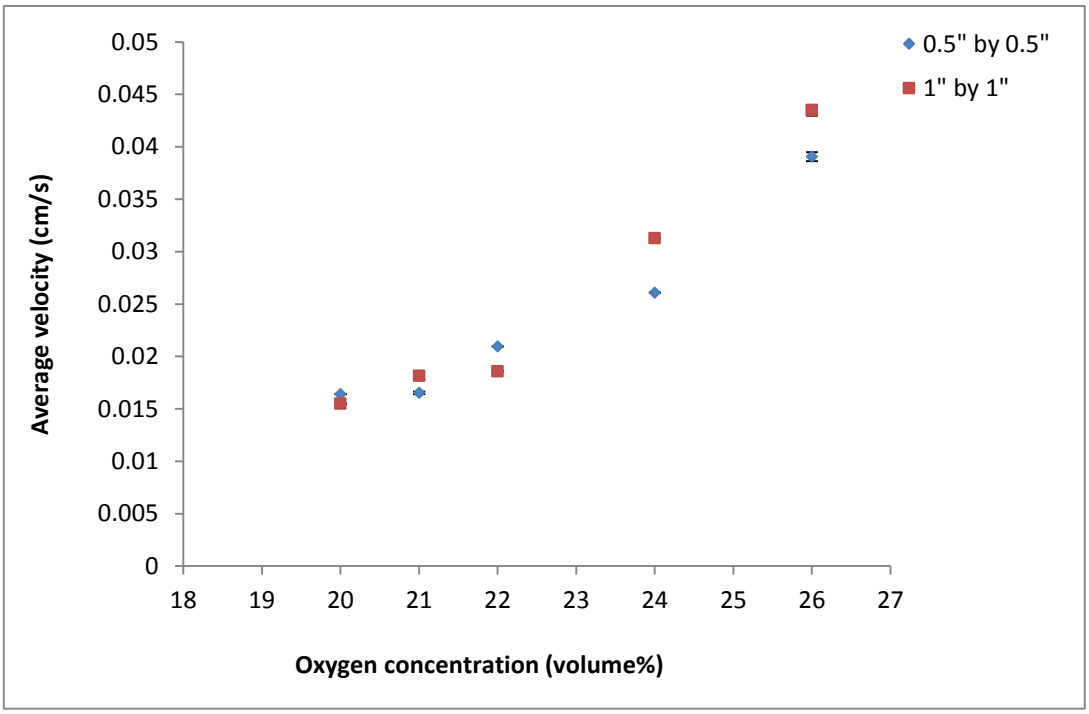

Figure 5.11 Flame spread rate versus oxygen concentration for different square rod dimensions.

The comparison between the flame spread rate and oxygen concentration for different dimensions (0.5×0.5 and 1×1 in) of square rods shows that the flame spread increases with an increase of oxygen concentrations for each dimension of square rods. Square rods with 1×1 in dimension need much more time to burn than 0.5×0.5 in square rods because they have a big surface area and more mass to burn. In accordance with this, a 1×1 in square rod would have a higher value of flame spread rate than a 0.5×0.5 square rod, especially at high oxygen concentrations (24 and 26%). Samples at 21% and 26% of oxygen concentration were burned three times to minimize the error. However, the flame spread rate at (20 and 22%) of oxygen concentrations for a square rod with 1×1 in was smaller than a square rod with 0.5×0.5 in dimensions. The summary of this comparison is a direct relationship between the flame spread and oxygen concentration. In other words, the flame spread rate for square rods with different dimensions increases as long as oxygen concentrations increase. (The results are shown in appendix C.1 and C.2).

5.4. Effect of Ambient Oxygen Concentrations on Angle of Pyrolysis for Different Square Rods

5.4.1. Effect of Ambient Oxygen Concentrations on Angle of Pyrolysis for a Square Rod with 0.5×0.5 inch Dimensions

The angle of pyrolysis, as shown in Fig. 5.12, decreases with oxygen concentration. The angle of pyrolysis reaches a high value (82.3°) at the smallest oxygen concentration (20%), and vice versa (at 26% is 51.2°). As long as the oxygen concentrations increase the material will burn faster, which causes a decrease in the angle of pyrolysis.

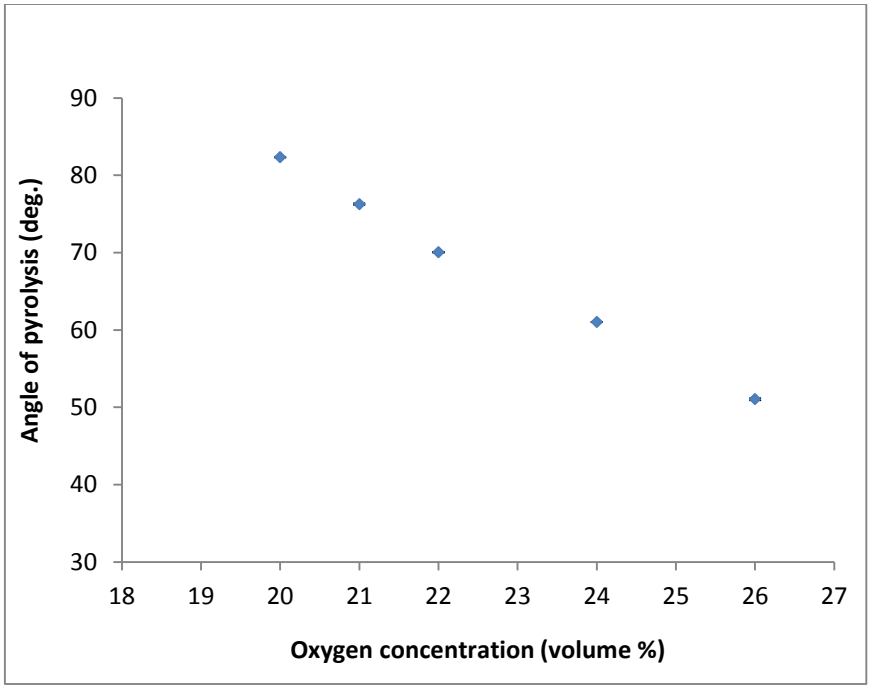

Figure 5.12 Angle of pyrolysis versus oxygen concentration for 0.5×0.5 in square rod.

5.4.2. Effect of Ambient Oxygen Concentrations on Angle of Pyrolysis for a Square Rod with 1*1 inch Dimensions

It can be seen in Fig. 5.13 how the angle of pyrolysis increases with decreasing oxygen concentrations, even if a square rod has 1×1 in dimensions. At low concentrations of oxygen, such as 20%, the angle of pyrolysis reaches the highest value, which is 68.3°, while the lowest value of the angle of pyrolysis is 33.1° at the highest oxygen concentrations, which is 26%. The values of the angle of pyrolysis are 58.1, 55.1 and 43.1° at 21, 2 and 24% of oxygen concentration, respectively.

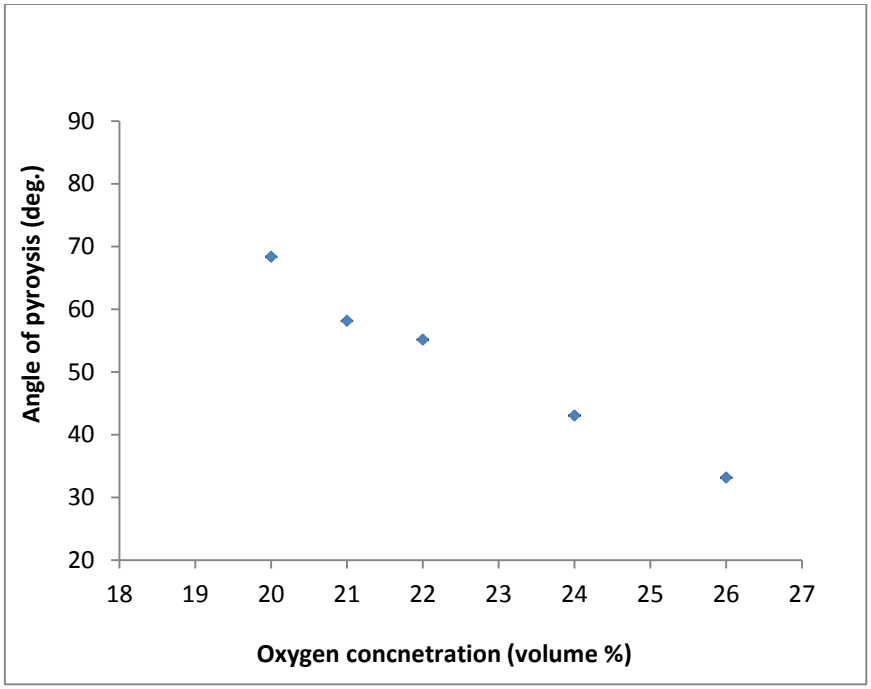

Figure 5.13 Angle of pyrolysis versus oxygen concentration for 1×1 in square rod.

5.4.3. The Comparison between Oxygen Concentrations and Flame Spread Rate for Different Dimensions of Square Rods (0.5×0.5 and 1×1 inch).

This comparison was made when they both burn until the same marked position .Fig 5.14 shows that the angles of pyrolysis in a 0.5×0.5 inch square rod are bigger than square rods with 1×1 in dimensions at different oxygen concentrations because of the surface area of the materials, which is bigger in 1×1 in than 0.5×0.5 inch square rods. As a result, it takes much time to burn and spread the flame onto the sides of the materials. Once the flame reaches to 1×1 in dimensions sides of the materials, the angle of pyrolysis starts to be clear to measure and it is smaller than a 0.5×0.5 inch angle for all oxygen concentrations. The spreading of flame from the middle to the sides is faster on the square rods with 0.5×0.5 inch dimension than those which have 1×1 inch dimension because of the same reason, which is its surface area. The conclusion of measuring the angles of pyrolysis for square rods with different dimensions at different oxygen concentrations is that the angle of pyrolysis is inversely proportional to the oxygen concentrations, which agrees with the conclusion of using sheets with different thicknesses at the same conditions. (The results are shown in appendix C.1 and C.2)

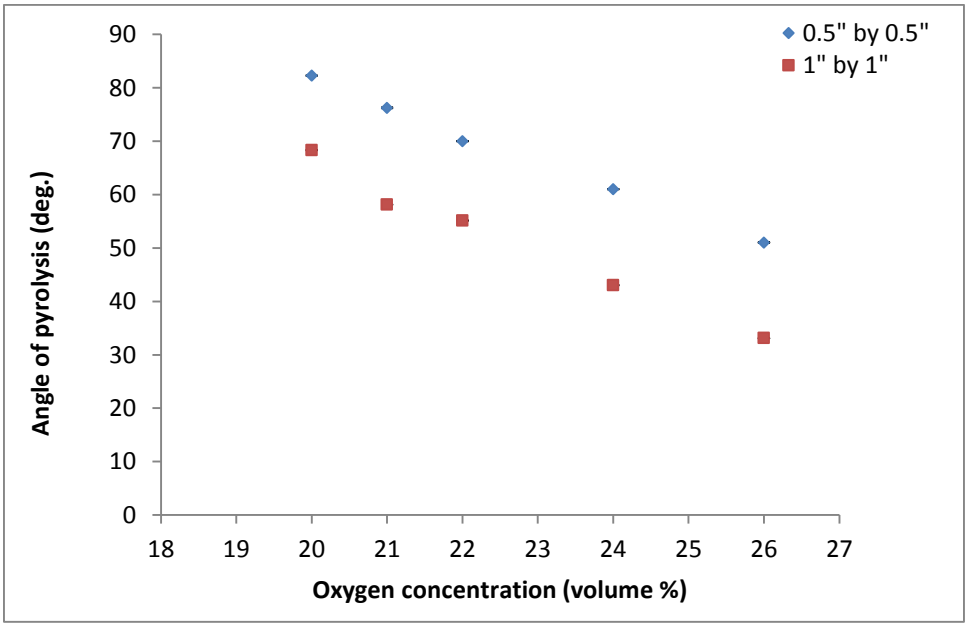

Figure 5.14 Angle of pyrolysis versus oxygen concentration for different square rod dimensions.

5.5. Effect of Ambient Oxygen Concentrations on Flame Spread Rate for Rods with Different Diameters (0.5 and 1 inch)

5.5.1. Effect of Ambient Oxygen Concentrations on Flame Spread Rate for Rods with a 0.5 inch Diameter.

The third kind of material used in the experiments was a rod with a different diameter. Fig. 5.15 below represents the relationship between the flame spread rate and oxygen concentration for rods with a 0.5 in diameter. The flame spread rate is nearly the same at 20 and 21% of oxygen concentration, which is (0.0079 and 0.0081 cm/s), respectively. The flame spread starts to go up regularly with the increasing of oxygen concentration to reach to the highest value (0.0178 cm/s) at 26% of oxygen concentration while the flame spread rate is 0.0098 and 0.0129 cm/s at 22 and 24% of oxygen concentrations.

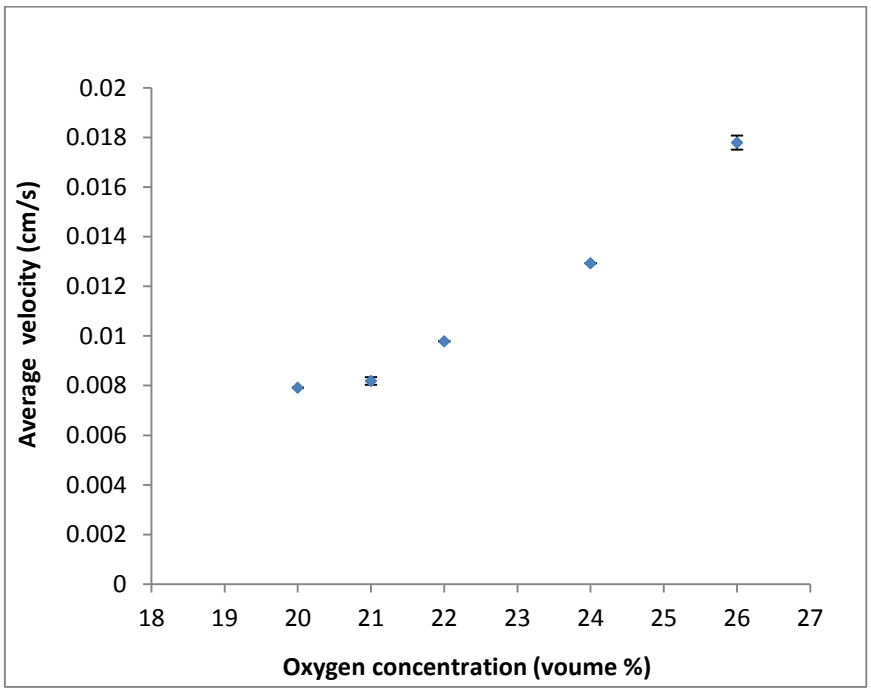

Figure 5.15 Flame spread rate versus the oxygen concentration for 0.5 in rod diameter.

5.5.2. Effect of Ambient Oxygen Concentrations on Flame Spread Rate for Rods with a 1-inch Diameter

The spreading of flames on rods with a 1 in diameter under the same conditions, which are used for rods 0.5 in diameter, is shown in Fig. 5.16. It is shown that there is a direct relationship between the flame spread rate and the oxygen concentration. In other words, the flame spread rate grows as long as the oxygen concentrations grow to be (0.0070, 0.0074 and 0.0085 cm/s) at (20, 21 and 22%) of oxygen concentrations, whereas the flame spread rate peaks with a high concentration of oxygen (24 and 26%) to be (0.0111 and 0.0147 cm/s).

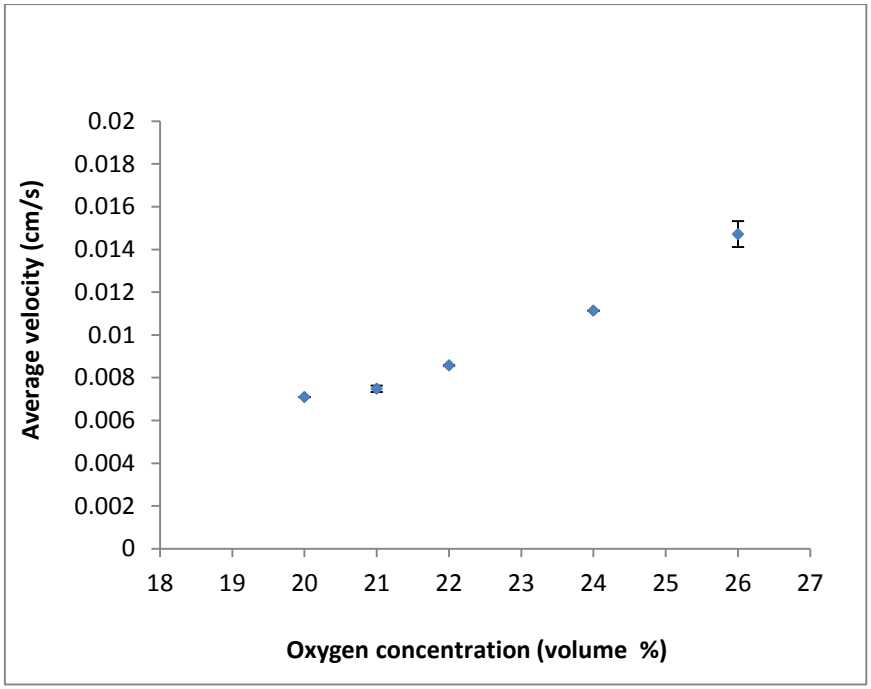

Figure 5.16 Flame spread rate versus the oxygen concentration for 1 in rod diameter.

5.5.3. The Comparison of Flame Spread Rate on Rods from PMMA with Different Diameters (0.5 and 1 inch) at Different Oxygen Concentrations

The flame spread rate on a 0.5 in diameter rod is faster than a 1 in diameter rod because of the same reasons that are mentioned before, which is a surface area. The surface area for the rods which have a big diameter (1 in) is bigger than for a 0.5 in diameter rod surface area. As a consequence, it takes more time to burn, which causes the highest velocities (flame spread rate). The flame spread rate on rods with different diameters (0.5 and 1 in) was found to be smaller than the flame spread rate on sheets with different thicknesses and square rods with different dimensions because of their shape. (The results are shown in appendix D.1 and D.2)

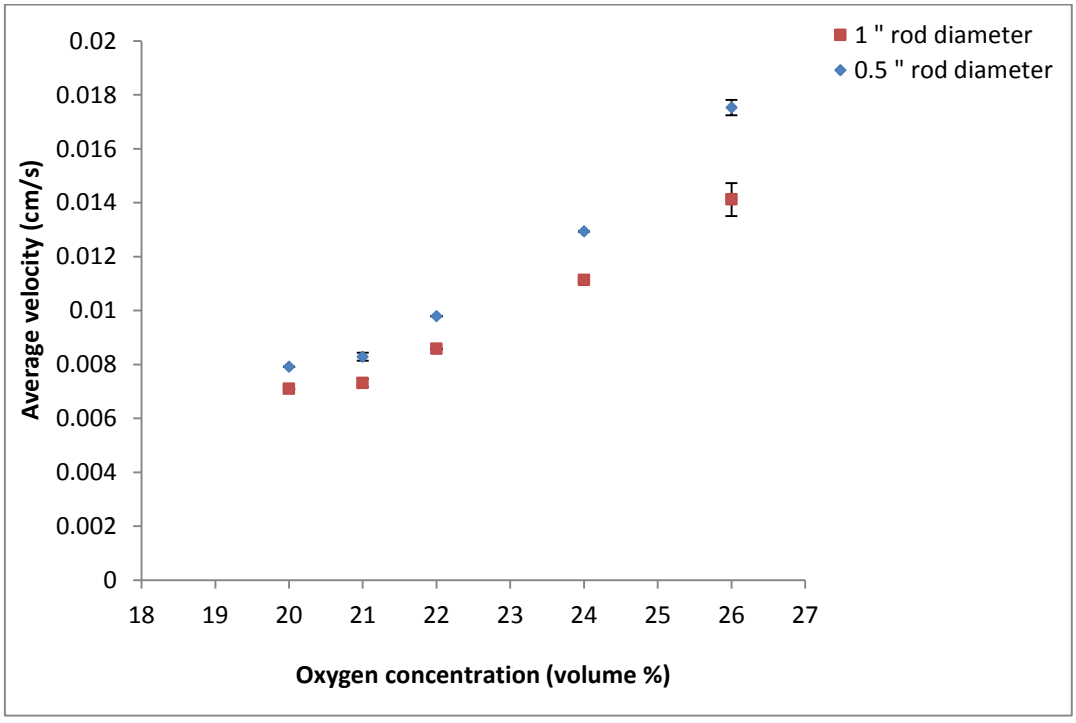

Figure 5.17 Flame spread rate versus oxygen concentration for rod with different diameters.

5.6. Effect of Ambient Oxygen Concentration on the Angle of Pyrolysis for Rods of PMMA with Different Diameters (0.5 and 1 inch)

5.6.1. Effect of Ambient Oxygen Concentration on Angle of Pyrolysis for 0.5 and 1 in Diameter Rods of PMMA

The angle of pyrolysis was not clear on rods of PMMA therefore, they were not measured by used same software. As a result of that, some calculations have been done to measure the angle of pyrolysis, as mentioned in 4.5.

Fig 5.18 below shows the angle of pyrolysis for 0.5 and 1 inch diameters of PMMA rod have been burned at different oxygen concentrations. The angle of pyrolysis almost decreases as the oxygen concentration increases and it has a big value at smallest oxygen concentration percentage was used. (The results are shown in appendix D.1 and D.2)

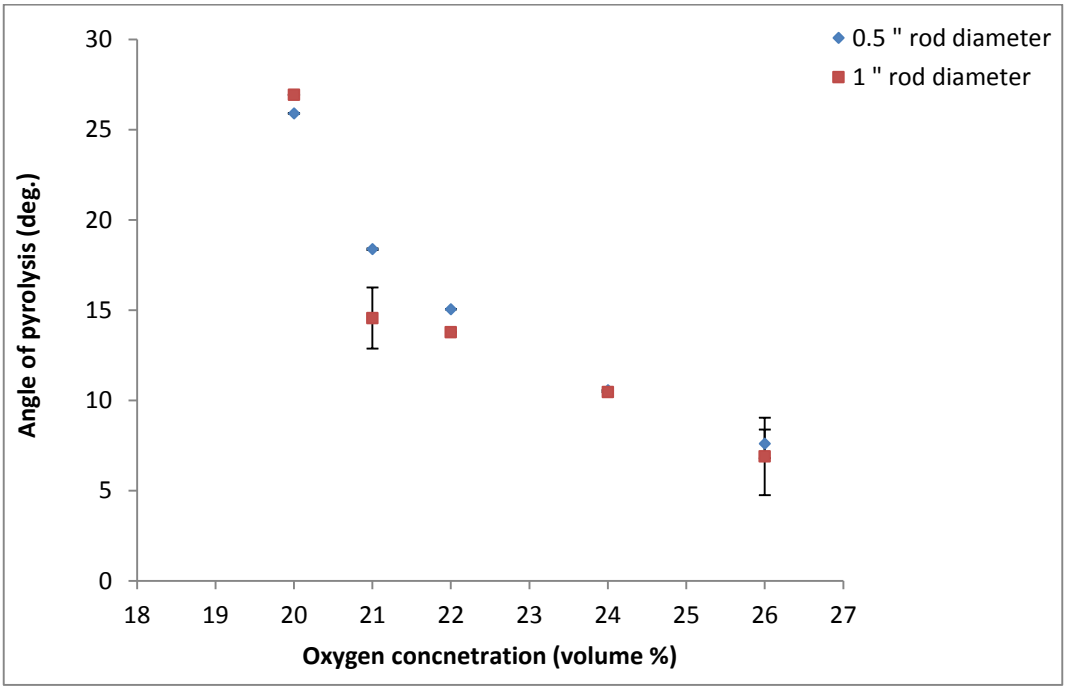

Figure 5.18 Angle of pyrolysis versus oxygen concentration for rods with different diameters.

5.6.2. The Comparison of Flame Spread Rate on Different Shapes of PMMA Material (sheet, square bar and rods) at Different Oxygen Concentrations

As mentioned above, the flame spread rates were calculated at three points on the samples for sheets and square bar while it is calculated at just two points which are on sides for rods Fig 5.19 shows a direct relationship between the flame spread rate and oxygen concentration for sheets, square bars and rods samples. Rod samples have smaller flame spread rates than sheets and square bar material because it has been calculated at two points on the samples and they have small surface area too.

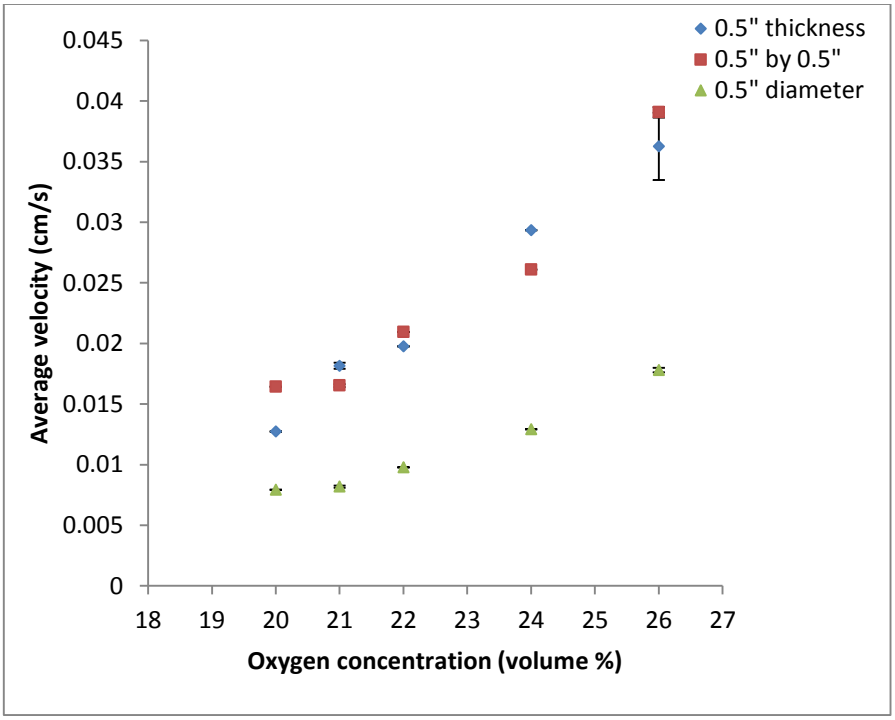

Figure 5.19 Flame spread rate versus oxygen concentration for different shapes of material (sheet, square bar and rod).

5.7. The Comparison of an angle of Pyrolysis on Different Shapes of PMMA Material (Sheet, square bar and rods) at Different Oxygen Concentrations

Fig. 5.20 shows an inverse relationship between the angle of pyrolysis and oxygen concentration. Square bar samples were burned faster than sheets and rod therefore, they have big angles of pyrolysis at different oxygen concentrations. On other hand, the rod samples take too much time to burn and the angle of pyrolysis was not clear and it could not be calculated by the software. It however has been calculated by using some calculations which are mentioned in experimental method chapter.

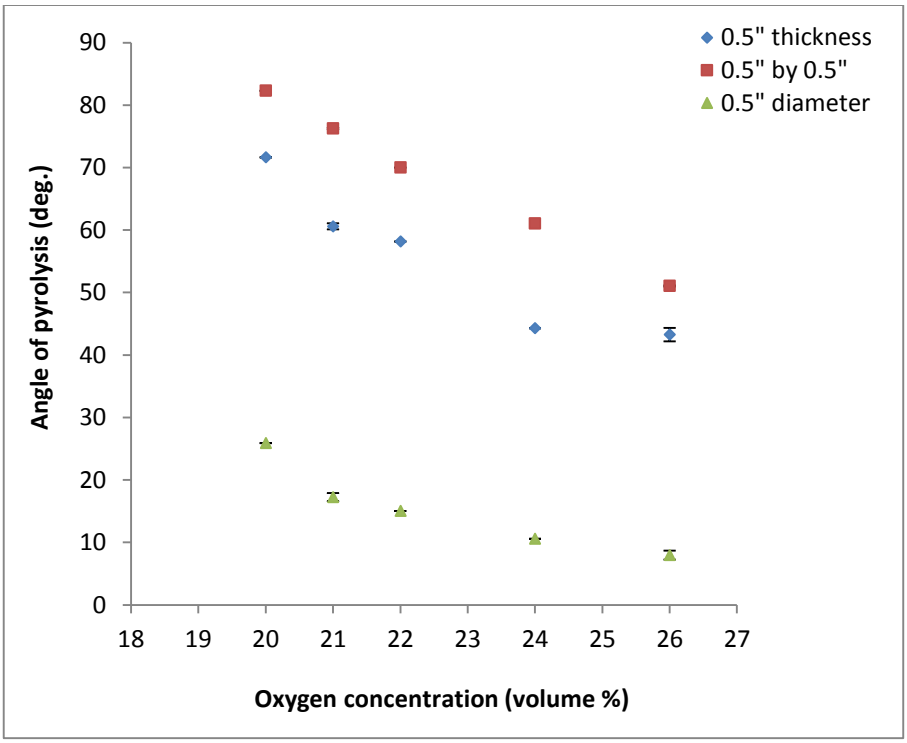

Figure 5.20 Angle of pyrolysis versus oxygen concentration for different shapes of material (sheet, square bars and rod).

5.8. Comparison Some of the Present Work , Especially Sheet with 0.25 in Thickness Burns at 21% Oxygen Concentration, with Ayani's work

Most of the previous work did not include different oxygen concentration. Therefore, the oxygen concentration did not mention in Ayani's work but he addressed his work (Downward flam spread over PMMA sheets in quiescent air). Figure 5.21 and 5.22 show the flame spread rate and the angle of pyrolysis at 21% oxygen concentration for sheet with 0.25 in thickness for both works (present and Ayani work). The flame spread rate and angle of pyrolysis at the present work looks to be bigger than the flame spread rate and angle of pyrolysis at Ayani's work. Some of reasons could be given a logical conclusion which are the oxygen concentration (21%) was accurate and considered in our work on the contrary, for Ayani's work which did not mention how he measured the oxygen concentration. Moreover, the PMMA materials which are used in Ayani and present work may have some different properties and came from different sources which is leading to have different flame spread rate and angle of pyrolysis at the concentration of the oxygen.

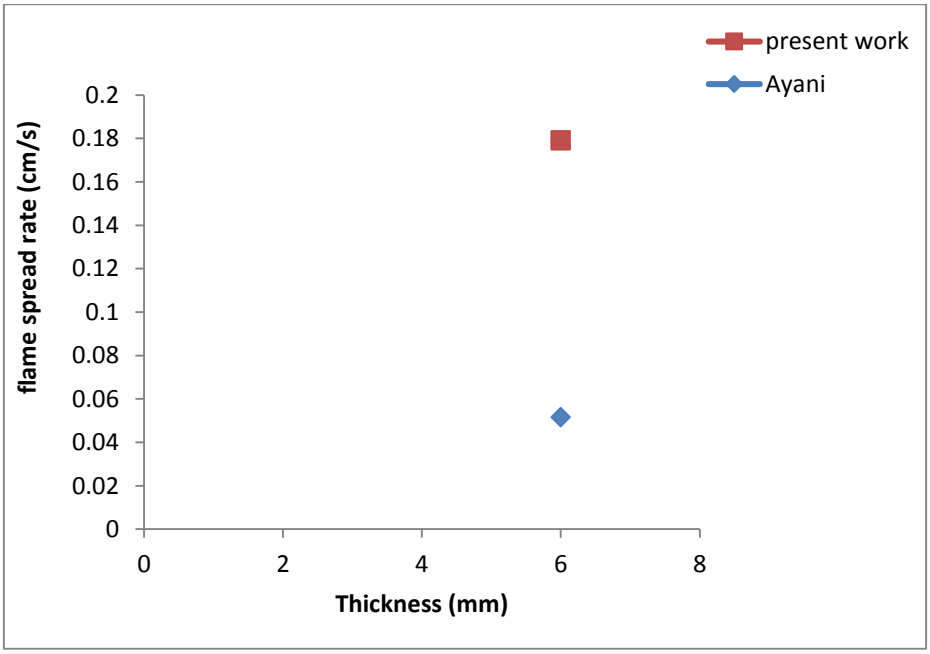

Figure 5.21 Comparison between Ayani and present work for flame spread rate for sheets with 0.25 in thickness at 21% oxygen concentration.

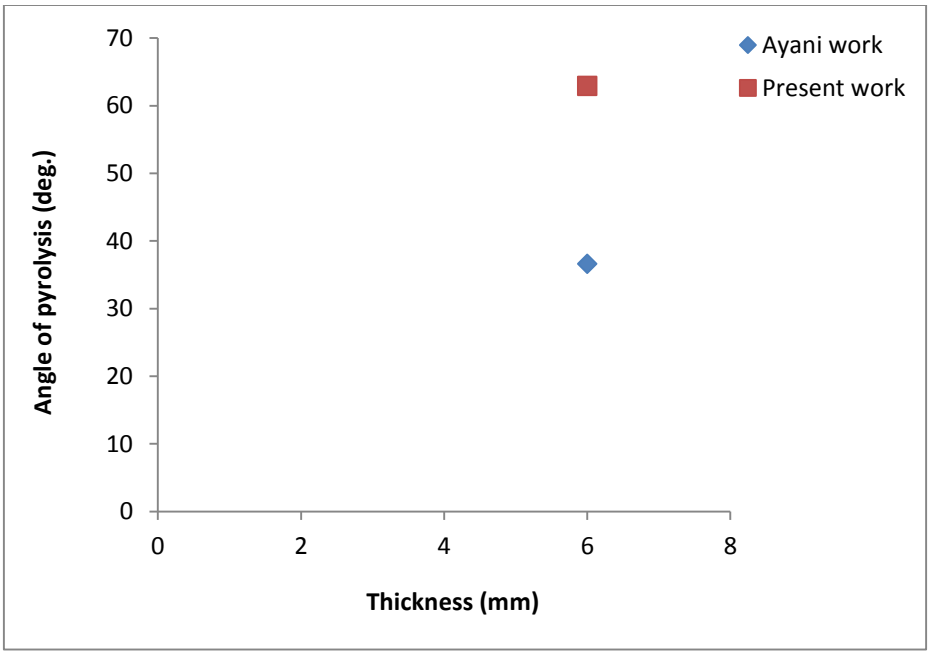

Figure 5.22 Comparison between Ayani and present work for angle of pyrolysis for sheets with 0.25 in thickness at 21% oxygen concentration.

Chapter 6 Conclusions and Future Work

The goal of this work was to experimentally study a downward flame spread rate and an angle of pyrolysis for different shapes (sheets, square bars and rods) of PMMA (polymethylmethacrylate) with variations in ambient oxygen concentrations by using a modified Critical Oxygen Index Apparatus. Also, the importance of this work is summarized in how the shape of the fuel plays an important role in the flame rate spreading and how the angle of pyrolysis looks through the spreading of the flame.

The results obtained from this work were:

1. The surface area of the fuel plays an important role in combustion process time and the angle of pyrolysis. Therefore, the materials which have a large surface area would have small values of the angle of pyrolysis and would take a lot of time to burn.
2. The average velocity, which represents the flame spreading rate, increases as the oxygen concentration increases.
3. The angle of pyrolysis, which represents the transition line on fuel sides, decreases as the oxygen concentration increases.
4. The angle of pyrolysis and the average velocity are almost constant for each oxygen concentration.

For future work, I would like to recommend some investigations:

1. A simulation of the downward spreading flame in the same condition and using the same fuel type to validate this work.
2. Compare between two fuel types in the same condition to see the effect of fuel type and study downward flame spread phenomena.
3. Study the comparison between different PMMA samples from different sources and burn them at the same conditions.

References

Alghamdi, A. (2012). *Measurement of gas temperature field in a flame spreading over solid fuel. MSc thesis.* San Diego State University).

Ayani, M. B., Esfahani, J. A., & Mehrabian, R. (2006). Downward flame spread over PMMA sheets in quiescent air: Experimental and theoretical studies. *Fire Safety Journal, 41*(2), 164-169. doi:http://dx.doi.org/10.1016/j.firesaf.2005.12.003

Bhattachariee, S., King, M. D., Takahashi, S., Nagumo, T., & Wakai, K. (2000). Downward flame spread over poly(methyl)methacrylate. *Proceedings of the Combustion Institute, 28*(2), 2891-2897. doi:http://dx.doi.org/10.1016/S0082-0784(00)80713-4

Bhattacharjee, S., & Altenkirch, R. A. (1992). A comparison of theoretical and experimental results in flame spread over thin condensed fuels in a quiescent, microgravity environment. *Symposium (International) on Combustion, 24*(1), 1669-1676. doi:http://dx.doi.org/10.1016/S0082-0784(06)80195-5

Bhattacharjee, S., West, J., & Dockter, S. (1996). A simplified theory for de ris flame over thick and thin fuel beds. *Combustion and Flame, 104*(1–2), 66-80. doi:http://dx.doi.org/10.1016/0010-2180(95)00109-3

De Ris, J. N. (1969). Spread of a laminar diffusion flame. *Symposium (International) on Combustion, 12*(1), 241-252. doi:http://dx.doi.org/10.1016/S0082-0784(69)80407-8

Delichatsios, M. A. (1986). Exact solution for the rate of creeping flame spread over thermally thin materials. *Combustion Science and Technology, 44*(5-6), 257-267. doi:10.1080/00102208608960307

Feldman, D. (1991). Properties of polymers, 3rd edition, by D. W. van krevelen, elsevier science publishers, amsterdam, oxford, new york, 1990,875 pages. *Journal of Polymer Science Part B: Polymer Physics, 29*(13), 1654-1654. doi:10.1002/polb.1991.090291313

Fernandez-Pello, A., & Williams, F. A. (1975). Laminar flame spread over PMMA surfaces. *Symposium (International) on Combustion, 15*(1), 217-231. doi:http://dx.doi.org/10.1016/S0082-0784(75)80299-2

Fernández-pello, A., & Williams, F. A. (1977). A theory of laminar flame spread over flat surfaces of solid combustibles. *Combustion and Flame, 28*(0), 251-277. doi:http://dx.doi.org/10.1016/0010-2180(77)90032-3

Fernandez-Pello, A. C., Ray, S. R., & Glassman, I. (1981). Flame spread in an opposed forced flow: The effect of ambient oxygen concentration. *Symposium (International) on Combustion, 18*(1), 579-589. doi:http://dx.doi.org/10.1016/S0082-0784(81)80063-X

Fernandez-Pello, A. C., & Santoro, R. J. (1979). On the dominant mode of heat transfer in downward flame spread. *Symposium (International) on Combustion, 17*(1), 1201-1209. doi:http://dx.doi.org/10.1016/S0082-0784(79)80114-9

Fernandez-Pello, A. C., & Hirano, T. (1982). Controlling mechanisms of flame spread. *Fire Science and Technology, 2*(1), 17-54. doi:10.3210/fst.2.17

Frey Jr., A. E., & T'ien, J. S. (1976). Near-limit flame spread over paper samples. *Combustion and Flame, 26*(0), 257-267. doi:http://dx.doi.org/10.1016/0010-2180(76)90076-6

Frey Jr., A. E., & T'ien, J. S. (1979). A theory of flame spread over a solid fuel including finite-rate chemical kinetics. *Combustion and Flame, 36*(0), 263-289. doi:http://dx.doi.org/10.1016/0010-2180(79)90064-6

Hirano, T., Noreikis, S. E., & Waterman, T. E. (1974). Measured velocity and temperature profiles near flames spreading over a thin combustible solid. *Combustion and Flame, 23*(1), 83-96. doi:http://dx.doi.org/10.1016/S0010-2180(74)80029-5

Ito, A., & Kashiwagi, T. (1988). Temperature measurements in PMMA during downward flame spread in air using holographic interferometry. *Symposium (International) on Combustion, 21*(1), 65-74. doi:http://dx.doi.org/10.1016/S0082-0784(88)80232-7

'Jellinek, H. H. G. (1968). Thermal degradation of PMMA. *Energies of Activation,*

Lastrina, F. A., Magee, R. S., & McAlevy III, R. F. (1971). Flame spread over fuel beds: Solid-phase energy considerations. *Symposium (International) on Combustion, 13*(1), 935-948. doi:http://dx.doi.org/10.1016/S0082-0784(71)80094-2

Nobuyuki Higashi, H. S. (1989). Thermal degradation of poly(methyl methacrylate): Polymer with head to head linkages. *Macromolecules, 22*, 4652-4654.

Ohki, Y., & Tsuga, S. (1974). On the flame spreading over a polymer surface. *Combustion Science and Technology, 9*(1-2), 1-12. doi:10.1080/00102207408960329

Parker, W. J. (1972). Flame spread model for cellulose materials. *Journal of Fire and Flammability, 3*, 254-269.

Wichman, I. S., & Williams, F. A. (1983). A simplified model of flame spread in an opposed flow along a flat surface of a semi-infinite solid. *Combustion Science and Technology, 32*(1-4), 91-123. doi:10.1080/00102208308923654

Wu, K. K., Fan, W. F., Chen, C. H., Liou, T. M., & Pan, I. J. (2003). Downward flame spread over a thick PMMA slab in an opposed flow environment: Experiment and modeling. *Combustion and Flame, 132*(4), 697-707. doi:http://dx.doi.org/10.1016/S0010-2180(02)00520-5

Zeus Industrial Products, I. (2005). Thermal degradation of plastics. *Technical WhitePaper,*

Appendices

Appendix A: Example of the calculations on 0.25 inch sheet thickness at 20% of oxygen concentration by using ImageJ software which is mentioned in 4.4.

Table A.1 The results from image analysis when flame starts to spread on the sample at image 35.

Time	**Length (cm)**			**Velocity (cm/s)**			**Average velocity**
(s)	1	2	3	1	2	3	**(cm/s)**
480	4.4	4.4	5.5	0.0091	0.0091	0.0114	0.0099

Total time = 840s

Burning Time = 360s

Delta time = 480s

Angle of pyrolysis = 71°

Table A.2 The results from image analysis when flame spreads on the sample at image 38

Time	**Length (cm)**			**Velocity (cm/s)**			**Average velocity**
(s)	1	2	3	1	2	3	**(cm/s)**
450	4.1	4.0	5.2	0.0091	0.0088	0.0115	0.0098

Total time = 840s

Burning time = 390s

Delta time = 450s

Angle of pyrolysis = 70.5°

Table A.3 The results from image analysis when flame spreads on the sample at image 41.

Time	**Length (cm)**			**Velocity (cm/s)**			**Average velocity**
(s)	1	2	3	1	2	3	**(cm/s)**
420	3.8	3.8	5.1	0.0090	0.0090	0.0121	0.0100

Total time = 840s

Burning time = 420s

Delta time = 420s

Angle of pyrolysis = 70.2°

Table A.4 The results from image analysis when flame spreads on the sample at image 44.

Time	**Length (cm)**			**Velocity (cm/s)**			**Average velocity**
(s)	1	2	3	1	2	3	**(cm/s)**
390	3.6	3.6	4.9	0.0092	0.0092	0.0125	0.0103

Total time = 480s

Burning time = 450s

Delta time = 390s

Angle of pyrolysis = 70°

Table A.5 The results from image analysis when flame spreads on the sample at image47.

Time (s)	Length (cm)			Velocity (cm/s)			Average velocity (cm/s)
	1	2	3	1	2	3	
360	3.2	3.2	4.6	0.0088	0.0088	0.0127	0.0101

Total time = 840s

Burning time = 480s

Delta time = 360

Angle of pyrolysis = 70°

Table A.6 The results from image analysis when flame spreads on the sample at image 50.

Time (s)	Length (cm)			Velocity (cm/s)			Average velocity (cm/s)
	1	2	3	1	2	3	
330	2.9	3	4.2	0.0087	0.0090	0.0127	0.0101

Total time = 840s

Burning time = 510s

Delta time = 330

Angle of pyrolysis = 70°

Table A.7 The results from image analysis when flame spreads on the sample at image 53.

Time	Length (cm)	Velocity (cm/s)	Average velocity

(s)	1	2	3	1	2	3	(cm/s)
300	2.6	2.8	3.9	0.0086	0.0093	0.013	0.0103

Total time = 840s

Burning time = 540s

Delta time = 300

Angle of pyrolysis = 70°

Table A.8 The results from image analysis when flame spreads on the sample at image 56.

Time (s)	Length (cm)			Velocity (cm/s)			Average velocity (cm/s)
	1	2	3	1	2	3	
270	2.5	2.5	3.8	0.0092	0.0092	0.0140	0.0108

Total time = 840s

Burning time = 570s

Delta time = 270

Angle of pyrolysis = 70°

Table A.9 Shows the angle of pyrolysis, average of velocity and burning time for 0.25 inch sheets thickness at 20% of oxygen concentration.

Image	Time (s)	Ave angle (deg.)	Ave velocity (cm/s)
35	360	71	0.0099
38	390	70.5	0.0098

41	420	70.2	0.0100
44	450	70	0.0103
47	480	70	0.0101
50	510	70	0.0102
53	540	70	0.0103
56	570	70	0.0108

Average angle of pyrolysis = 70.2°

Average of velocity = 0.01 cm/s

The tables from A.1 to A.9 were an example to show how the calculations are obtained from image analysis by using Imagej software.

Appendix B: The values of average velocity and angle of pyrolysis on sheets samples with different thicknesses.

Table B.1 PMMA sheets with 0.25 inch thickness.

O2 %	Ave angle (deg.)	Ave velocity (cm/s)
20	70.2	0.0103

21	62.9	0.0179
22	48.3	0.0251
24	47.3	0.0343
26	45.1	0.0505

Table B.2 PMMA sheets with 0.5 inch thickness.

O2 %	**Ave angle (deg.)**	**Ave velocity (cm/s)**
20	71.6	0.0127
21	60.7	0.0186
22	58.2	0.0198
24	44.3	0.0293
26	42.6	0.0381

Table B.3 PMMA sheets with 0.75 inch thickness.

O2 %	**Ave angle (deg.)**	**Ave velocity (cm/s)**
20	77.5	0.0119
21	63.9	0.0163
22	58.1	0.0186
24	48.1	0.0270
26	35.3	0.0379

Appendix C: The values of average velocity and angle of pyrolysis on square bar samples with different dimensions.

Table C.1 PMMA square bar 0.5×0.5 inch dimensions.

O2 %	**Ave angle (deg.)**	**Ave velocity (cm/s)**
20	82.3	0.0164

21	76.2	0.0165
22	70.0	0.0209
24	61.0	0.0261
26	51.2	0.0393

Table C.2 PMMA square bar with 1×1 inch dimensions.

Oxygen %	**Ave angle (deg.)**	**Ave velocity (cm/s)**
20	68.3	0.0155
21	58.1	0.0182
22	55.1	0.0186
24	43.1	0.0313
26	33.1	0.0432

Appendix D: The values of average velocity and angle of pyrolysis on rods samples with different diameters.

Table D.1 PMMA rod 0.5 inch diameter.

Oxygen %	**Ave angle (deg.)**	**Ave velocity (cm/s)**

20	25.9	0.0079
21	17.3	0.0082
22	15.1	0.0098
24	10.6	0.0129
26	8	0.0178

Table D.2 PMMA rod 1 inch diameter.

Oxygen Percentage %	Ave angle (deg.)	Ave velocity (cm/s)
20	28.2	0.0071
21	13.3	0.0075
22	17.4	0.0086
24	10.8	0.0111
26	9	0.0147

Appendix E: The standard deviation and the error bar for repetition cases at 21 and 26% of oxygen concentrations

Table E.1 Standard deviation of the average velocity for 0.25 in sheet thickness at 21% of oxygen concentration

image	Time (s)	Ave velocity 1 (cm/s)	Ave velocity 2 (cm/s)	Ave velocity 3 (cm/s)	STDV velocity (cm/s)
23	240	0.0162	0.0163	0.0165	0.000132447

26	270	0.0166	0.0166	0.0167	8.10514E-05
29	300	0.0170	0.0168	0.0169	0.000117818
32	330	0.0175	0.0171	0.0173	0.000221048
35	360	0.0181	0.0173	0.0173	0.000478009
38	390	0.0185	0.0176	0.0177	0.000507968
41	420	0.0191	0.0179	0.0180	0.000668976
44	450	0.0195	0.0184	0.0184	0.0006315
47	480	0.0201	0.0189	0.0191	0.000664952
50	510	0.0209	0.0194	0.0199	0.00076729

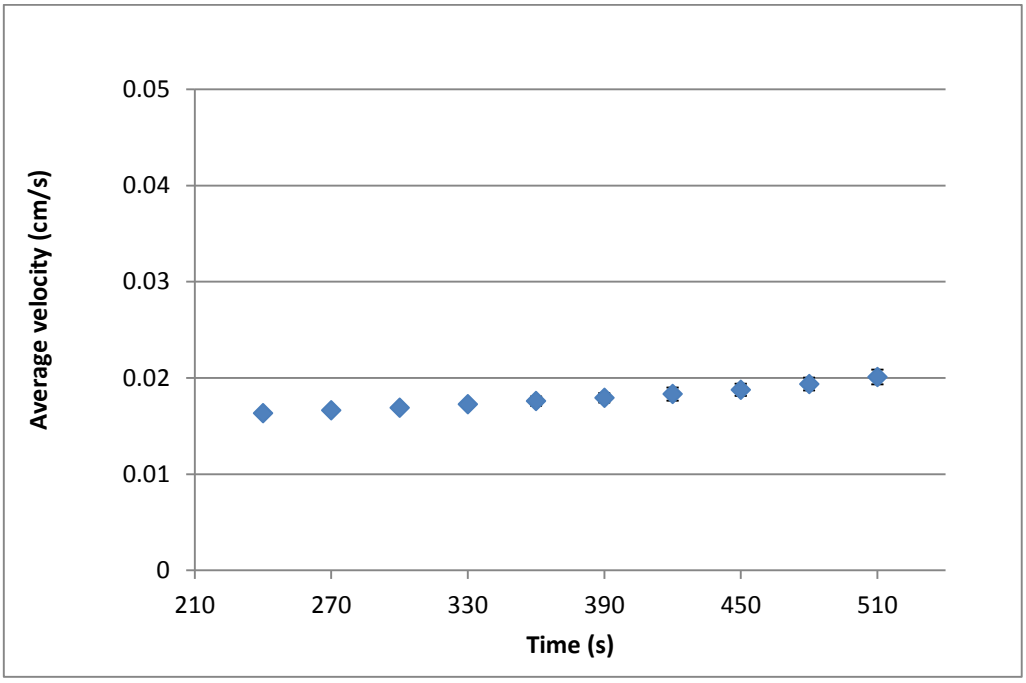

Figure E.1 time versus average velocity for 0.25 in sheet thickness at 21% oxygen concentration with error bar

Table E.2 Standard deviation of the average velocity for 0.25-in sheet thickness at 26% of oxygen concentration

Image	Time (s)	Ave velocity 1 (cm/s)	Ave velocity 2 (cm/s)	Ave velocity 3 (cm/s)	Ave velocity (cm/s)	STDV velocity (cm/s)
8	90	0.0369	0.0408	0.0471	0.0416	0.005132515
11	120	0.0376	0.0416	0.0526	0.0439	0.007762081

14	150	0.0409	0.0436	0.0613	0.0486	0.011107986
17	180	0.0418	0.0476	0.0761	0.0552	0.018341516
20	210	0.0443	0.0603	0.1136	0.0727	0.036274395

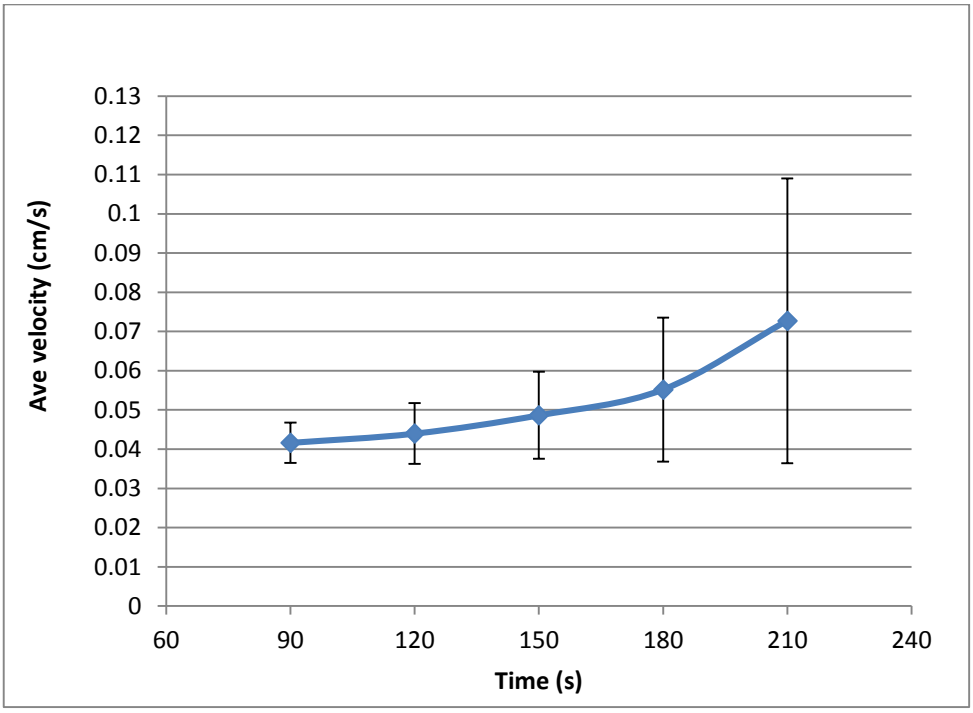

Figure E.2 time versus average velocity for 0.25 in sheet thickness at 26% oxygen concentration with error bar

Table E.3 Standard deviation of the average velocity for 0.5-in sheet thickness at 21% of oxygen concentration

Image	Time (s)	Ave velocity1 (cm/s)	Ave velocity2 (cm/s)	Ave velocity 3 (cm/s)	Average velocity (cm/s)	STDV velocity (cm/s)
29	300	0.0163	0.0163	0.0161	0.0162	0.00013578
32	330	0.0166	0.0169	0.0164	0.0166	0.000252095

35	360	0.0169	0.0169	0.0165	0.0168	0.000255862
38	390	0.0173	0.0173	0.0168	0.0172	0.000297658
41	420	0.0176	0.0176	0.0171	0.0175	0.000270567
44	450	0.0178	0.0178	0.0175	0.0177	0.000154888
47	480	0.0183	0.0183	0.0178	0.0182	0.000292616
50	510	0.0195	0.0192	0.0189	0.0192	0.00030108
53	540	0.0198	0.0198	0.0190	0.0195	0.000459426
56	570	0.0212	0.0212	0.0209	0.0212	0.000174706

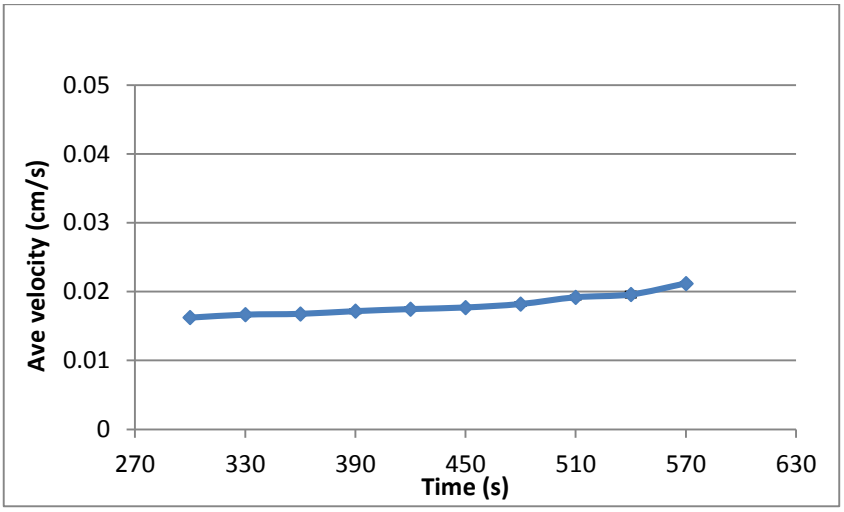

Figure E.3 time versus average velocity for 0.5 in sheet thickness at 21% oxygen concentration with error bar

Table E.4 Standard deviation of the average velocity for 0.5-in sheet thickness at 26% of oxygen concentration

Image	Time (s)	Ave velocity 1 (cm/s)	Ave velocity 2 (cm/s)	Ave velocity 3 (cm/s)	Ave velocity (cm/s)	STDV velocity (cm/s)
8	90	0.035	0.035	0.038	0.036	0.002092514

11	120	0.036	0.036	0.039	0.037	0.001892142
14	150	0.037	0.037	0.041	0.038	0.0026081
17	180	0.038	0.038	0.043	0.0395	0.002774539
20	210	0.041	0.041	0.046	0.043	0.00266797

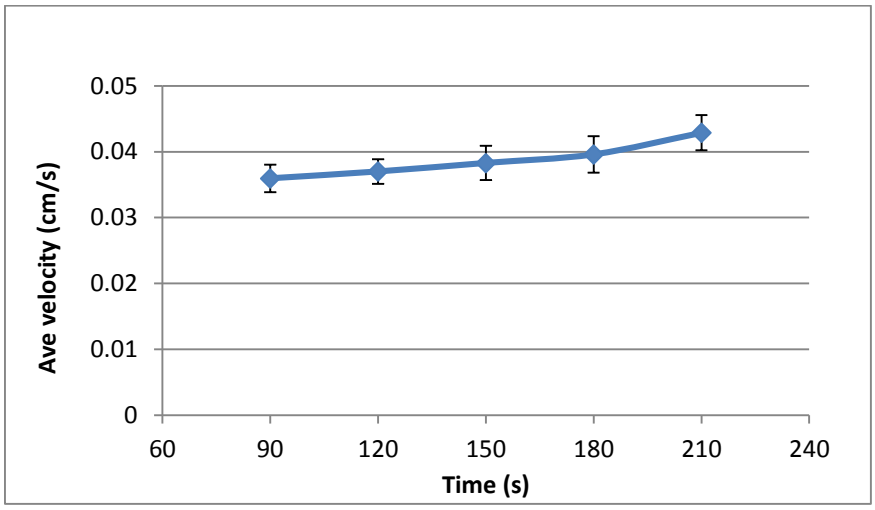

Figure E.4 time versus average velocity for 0.5 in sheet thickness at 26% oxygen concentration with error bar

Table E.5 Standard deviation of the average velocity for 0.75-in sheet thickness at 21% of oxygen concentration

Image	Time (s)	Ave velocity 1 (cm/s)	Ave velocity 2 (cm/s)	Ave velocity 3 (cm/s)	Ave velocity (cm/s)	STDV velocity (cm/s)
47	480	0.0155	0.0155	0.0139	0.0149	0.000953

50	510	0.0156	0.0160	0.0143	0.0153	0.000874
53	540	0.016	0.016	0.014	0.016	0.001108
56	570	0.017	0.017	0.015	0.016	0.001155
59	600	0.017	0.017	0.015	0.017	0.001121
62	630	0.018	0.018	0.016	0.018	0.001639
65	660	0.019	0.019	0.016	0.018	0.001605
68	690	0.020	0.020	0.017	0.019	0.001953

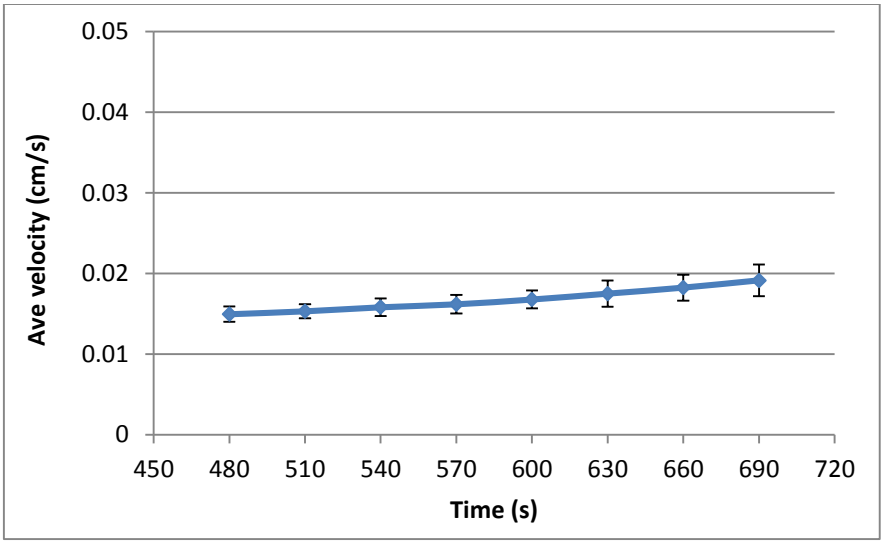

Figure E.5 time versus average velocity for 0.75 in sheet thickness at 21% oxygen concentration with error bar

Table E.6 Standard deviation of the average velocity for 0.75-in sheet thickness at 26% of oxygen concentration

Image	Time (s)	Ave velocity1 (cm/s)	Ave velocity 2 (cm/s)	Ave velocity3 (cm/s)	Ave velocity (cm/s)	STDV velocity (cm/s)

11	120	0.0369	0.0363	0.0377	0.0369	0.000727864
14	150	0.0371	0.0366	0.0379	0.0372	0.000676877
17	180	0.038	0.038	0.039	0.039	0.001127571
20	210	0.038	0.041	0.043	0.041	0.002682561

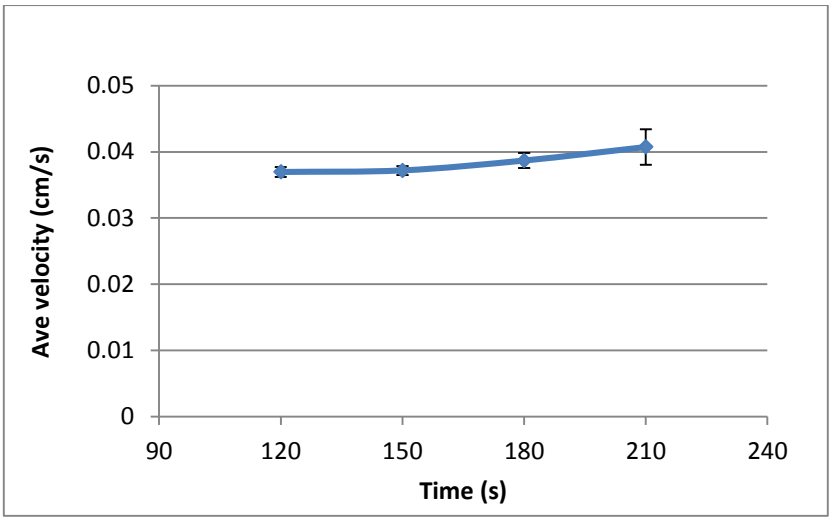

Figure E.6 time versus average velocity for 0.75 in sheet thickness at 26% oxygen concentration with error bar

Table E.7 Standard deviation of the average velocity for 0.5-in × 0.5-in square bar dimensions at 21% of oxygen concentration

Image	Time (s)	Ave velocity 1 (cm/s)	Ave velocity 2 (cm/s)	Ave velocity 3 (cm/s)	Ave velocity (cm/s)	STDV velocity (cm/s)
23	240	0.0161	0.0162	0.0159	0.0161	0.000164

26	270	0.0161	0.0163	0.0159	0.0161	0.000199
29	300	0.0162	0.0164	0.0160	0.0162	0.000216
32	330	0.0164	0.0164	0.0161	0.0163	0.000159
35	360	0.0165	0.0166	0.0163	0.0165	0.000191
38	390	0.0166	0.0167	0.0165	0.0166	0.000113
41	420	0.01661	0.01671	0.01664	0.01665	5.01E-05
44	450	0.0169	0.0169	0.0167	0.0169	0.000155
47	480	0.01725	0.01709	0.01719	0.01718	7.87E-05

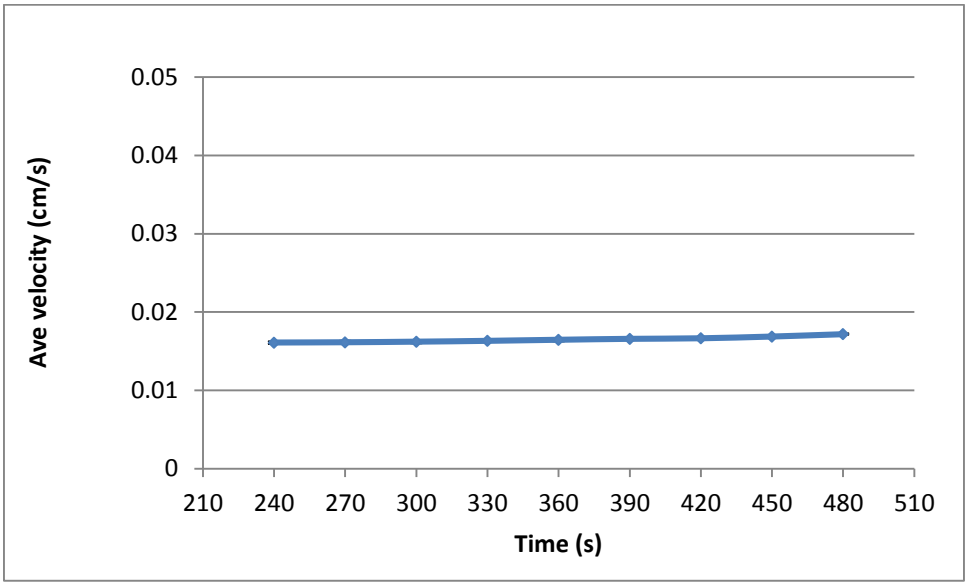

Figure E.7 time versus average velocity for 0.5×0.5 square bar dimensions at 21% of oxygen concentration

Table E.8 Standard deviation of the average velocity for 0.5-in × 0.5-in square bar dimensions at 26% of oxygen concentration

Image	Time (s)	Ave velocity 1 (cm/s)	Ave velocity 2 (cm/s)	Ave velocity 3 (cm/s)	Ave velocity (cm/s)	STDV velocity (cm/s)
5	60	0.0389	0.0395	0.0389	0.0391	0.000305563

8	90	0.0390	0.0397	0.0390	0.0392	0.000414834
11	120	0.0390	0.0398	0.0390	0.0393	0.000442663
14	150	0.0390	0.0399	0.0391	0.0393	0.000471908
17	180	0.0394	0.0404	0.0396	0.0398	0.000510718

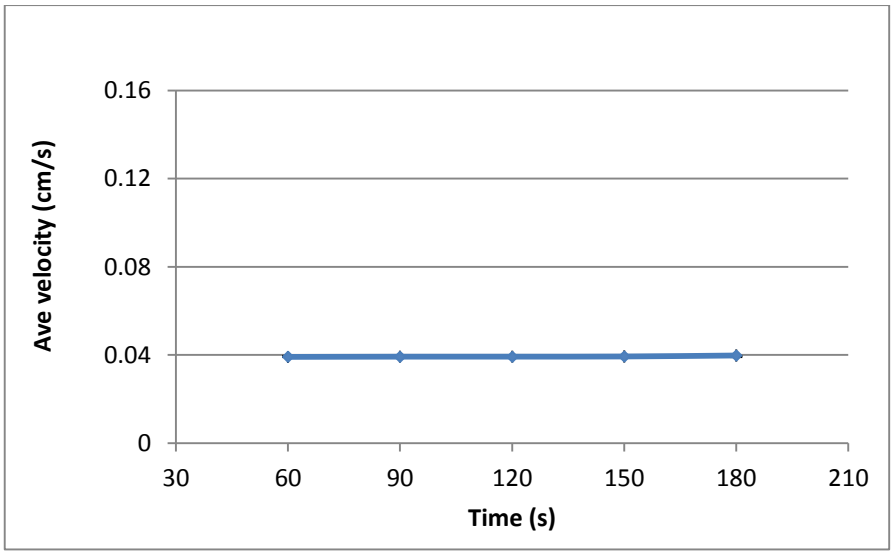

Figure E.8 time versus average velocity for 0.5×0.5 square bar dimensions at 26% of oxygen concentration

Table E.9 Standard deviation of the average velocity for 1-in × 1-in square bar dimensions at 21% of oxygen concentration

Image	Time (s)	Ave velocity 1 (cm/s)	Ave velocity 2 (cm/s)	Ave velocity 3 (cm/s)	Ave velocity (cm/s)	STDV velocity (cm/s)
23	240	0.0171	0.0175	0.0170	0.0172	0.000237464
26	270	0.0172	0.0176	0.0170	0.0173	0.000280707

29	300	0.0172	0.0176	0.0171	0.0173	0.000280444
32	330	0.0178	0.0179	0.0175	0.0178	0.000205899
35	360	0.0179	0.0182	0.0177	0.0179	0.000271899
38	390	0.0182	0.0187	0.0179	0.0183	0.000386432
41	420	0.0184	0.0188	0.0181	0.0185	0.00036433
44	450	0.0187	0.0191	0.0183	0.0187	0.000367609
47	480	0.0188	0.0194	0.0185	0.0189	0.000435146
50	510	0.0189	0.0196	0.0188	0.0191	0.000416173
53	540	0.0194	0.0199	0.0196	0.0196	0.000214262

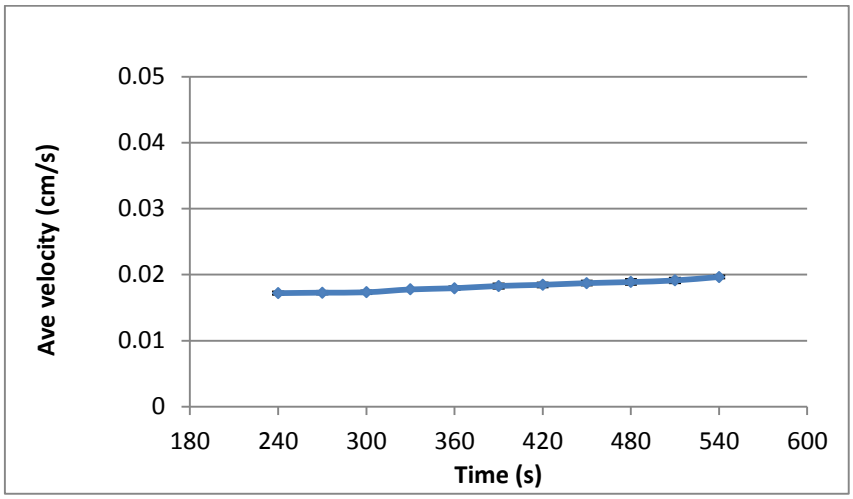

Figure E.9 time versus average velocity for 1×1 square bar dimensions at 21% of oxygen concentration

Table E.10 Standard deviation of the average velocity for 1-in × 1-in square bar dimensions at 26% of oxygen concentration

Image	Time (s)	Ave velocity 1 (cm/s)	Ave velocity 2 (cm/s)	Ave velocity 3 (cm/s)	Ave velocity (cm/s)	STDV velocity (cm/s)
11	120	0.0430	0.0421	0.043	0.0427	0.000506

14	150	0.0436	0.0427	0.0436	0.0433	0.000514
17	180	0.0439	0.0429	0.044	0.0436	0.000523

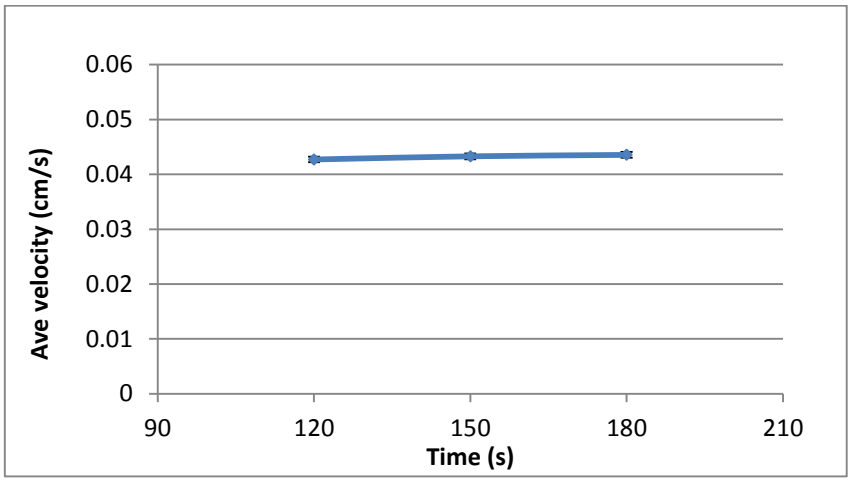

Figure E.10 time versus average velocity for 1×1 square bar dimensions at 26% of oxygen concentration

Table E.11 Standard deviation of the average velocity for 0.5-in diameter rod at 21% of oxygen concentration

Image	Time (s)	Ave velocity 1 (cm/s)	Ave velocity 2 (cm/s)	Ave velocity 3 (cm/s)	Ave velocity (cm/s)	STDV velocity (cm/s)
2	30	0.00774	0.00760	0.00771	0.00768	6.94612E-05
17	180	0.0078	0.00767	0.00780	0.00776	7.36777E-05

32	330	0.00799	0.00783	0.00785	0.00789	8.54975E-05
47	480	0.0081	0.0079	0.0080	0.0080	0.000105737
62	630	0.0084	0.0081	0.0081	0.0082	0.000153637
77	780	0.0089	0.0083	0.0083	0.0085	0.000355505
92	930	0.0091	0.0086	0.0087	0.0088	0.000266664
107	1080	0.0098	0.0091	0.0092	0.0093	0.00037718

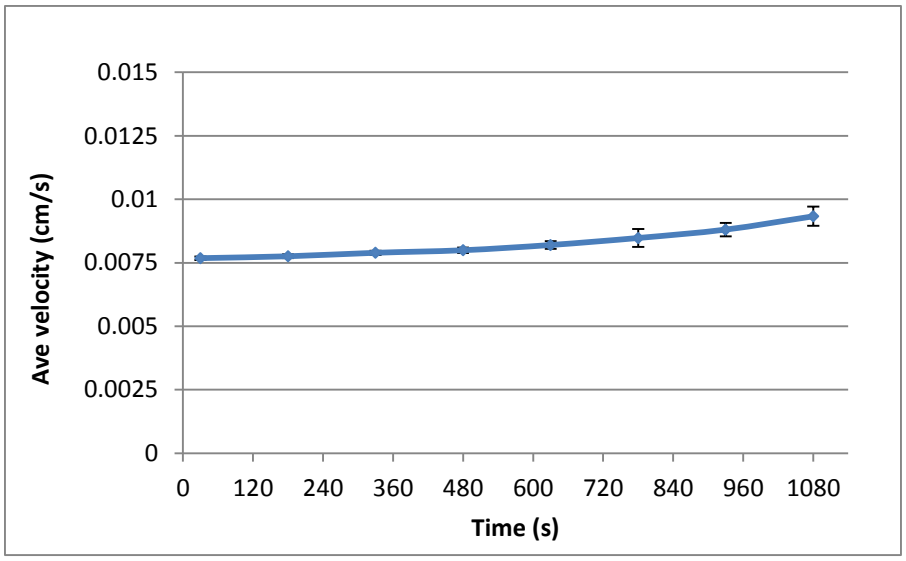

Figure E.11 time versus average velocity for 0.5 in diameter rod at 21% of oxygen concentration

Table E.12 Standard deviation of the average velocity for 0.5-in diameter rod at 26% of oxygen concentration

Image	Time (s)	Ave velocity 1 (cm/s)	Ave velocity 2 (cm/s)	Ave velocity 3 (cm/s)	Ave velocity (cm/s)	STDV velocity (cm/s)
2	30	0.0175	0.0184	0.0181	0.0180	0.000436836
7	80	0.0178	0.0183	0.0181	0.0180	0.000255883

12	130	0.0176	0.0181	0.0180	0.0179	0.000262024
17	180	0.0176	0.0180	0.0178	0.0178	0.000231665
22	230	0.0174	0.0180	0.0179	0.0178	0.000311305
27	280	0.0174	0.0180	0.0176	0.0177	0.000276468
32	330	0.0174	0.0180	0.0174	0.0176	0.000358876
37	380	0.0174	0.0180	0.0174	0.0176	0.000324615
42	430	0.0176	0.0188	0.0179	0.0181	0.000621784

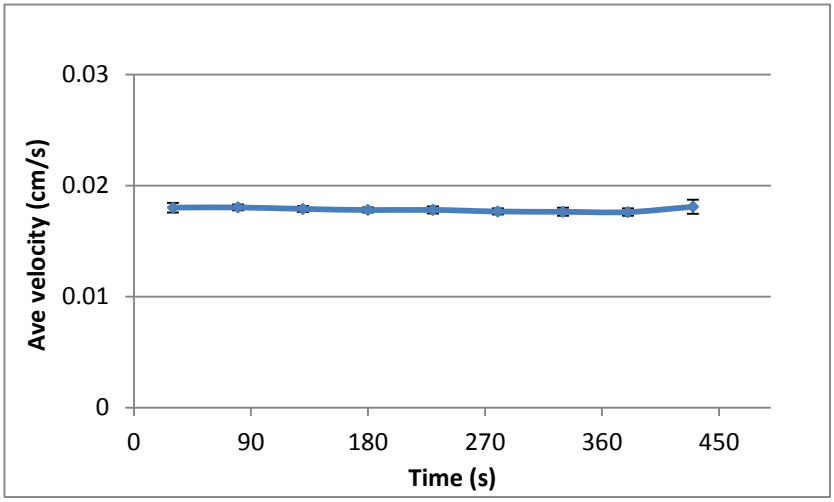

Figure E. 12 time versus average velocity for 0.5 in diameter rod at 26% of oxygen concentration

Table E.13 Standard deviation of the average velocity for 1-in diameter rod at 21% of oxygen concentration

Image	Time (s)	Ave velocity 1 (cm/s)	Ave velocity 2 (cm/s)	Ave velocity 3 (cm/s)	Ave velocity (cm/s)	STDV velocity (cm/s)
17	180	0.0067	0.0070	0.0071	0.0069	0.000183196

32	330	0.0070	0.0071	0.0072	0.0071	0.000113405
47	480	0.0071	0.0072	0.0074	0.0073	0.000145296
62	630	0.0072	0.0074	0.0075	0.0074	0.000176622
77	780	0.0075	0.0079	0.0077	0.0077	0.000175155
92	930	0.0077	0.0080	0.0079	0.0078	0.000152663
107	1080	0.0080	0.0084	0.0082	0.0082	0.000200264
122	1230	0.0086	0.0092	0.0086	0.0088	0.000334314

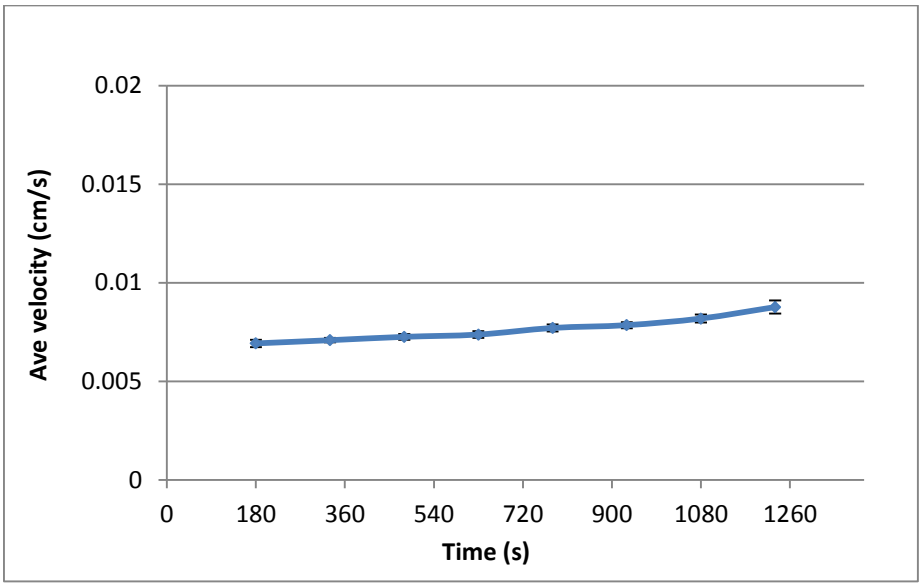

Figure E.13 time versus average velocity for 1 in diameter rod at 21% of oxygen concentration

Table E.14 Standard deviation of the average velocity for 1-in diameter rod at 26% of oxygen concentration

Image	**Time (s)**	**Ave velocity 1 (cm/s)**	**Ave velocity 2 (cm/s)**	**Ave velocity 3 (cm/s)**	**STDV velocity (cm/s)**

2	30	0.0144	0.0153	0.0150	0.000422378
7	80	0.0145	0.0156	0.0149	0.000405108
12	130	0.0144	0.0153	0.0148	0.000441147
17	180	0.0144	0.0155	0.0147	0.000537951
22	230	0.0145	0.0153	0.0147	0.000450853
27	280	0.0142	0.0153	0.0149	0.000584789
32	330	0.0138	0.0155	0.0146	0.000820206
37	380	0.0139	0.0155	0.0145	0.000796584
42	430	0.0139	0.0150	0.0147	0.00055975
47	480	0.0135	0.0154	0.0144	0.000949257
52	530	0.0136	0.0159	0.0147	0.001145765

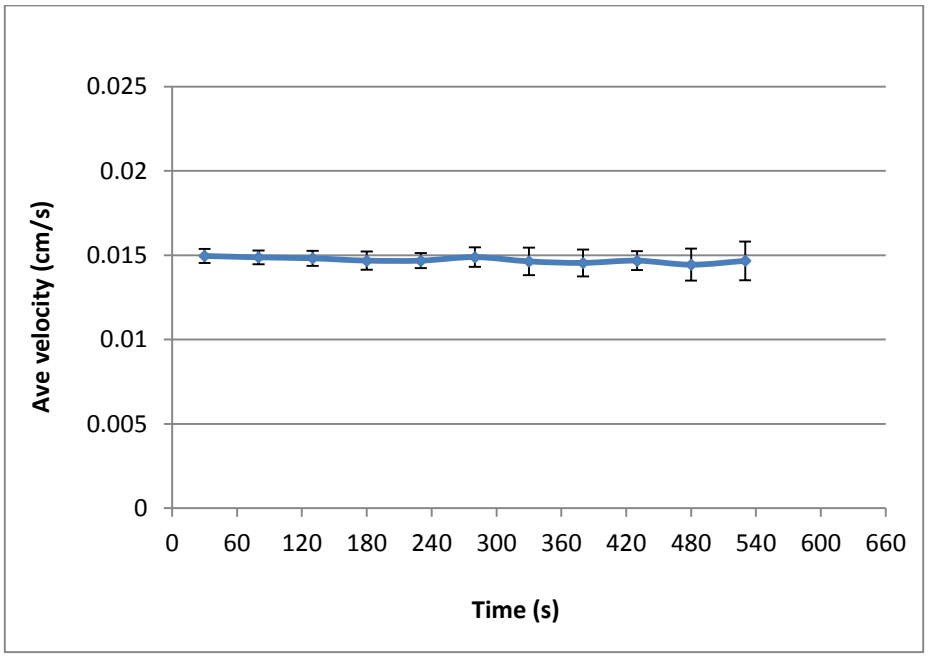

Figure E.14 time versus average velocity for 1 in diameter rod at 26% of oxygen concentration